

Kondo screening cloud effects in mesoscopic devices

Pascal Simon*

*Department of Physics and Astronomy, University of Basel, CH-4056 Basel, Switzerland
LEPES & LPM2C, CNRS, 25 av. des martyrs, 38042 Grenoble, France*

Ian Affleck[†]

Physics Department, Boston University, 590 Commonwealth Ave., Boston, MA02215

(Dated: November 17, 2018)

We study how finite size effects may appear when a quantum dot in the Kondo Coulomb blockade regime is embedded into a mesoscopic device with finite wires. These finite size effects appear when the size of the mesoscopic device containing the quantum dot is of the order of the size of Kondo cloud and affect all thermodynamic and transport properties of the Kondo quantum dot. We also generalize our results to the experimentally relevant case where the wires contain several transverse modes/channels. Our results are based on perturbation theory, Fermi liquid theory and slave boson mean field theory.

I. INTRODUCTION

In the last years, a large number of experiments have been realized in order to probe some theoretical predictions related to the Kondo effect. This has been made possible using small semiconductor quantum dots^{1,2,3} and also thin single wall carbon nanotubes.⁴ In these devices, it is expected that when the ground state of the quantum dot or of the thin carbon nanotubes has a spin $S = 1/2$ or equivalently when its last full level contains on average one electron and becomes degenerate, the dot plays the role of the Kondo impurity when embedded into conducting leads.

One of the major and still controversial issue in the Kondo physics concerns the Kondo screening cloud. The heuristic picture is that an electron in an extended wave function with a size of order $\xi_K = \hbar v_F / T_K$ (the Kondo length scale) surrounds the impurity, forming a singlet with it. The remaining electrons outside the cloud do not feel the impurity spin at low energies but rather a scattering potential, caused by the complex formed between the cloud and the impurity, resulting in a $\pi/2$ phase shift at the Fermi energy (some recent experiments by Heiblum *et al*⁵ have tried to measure this $\pi/2$ phase shift but obtain results in disagreement with theoretical predictions.⁶ Nevertheless, the issue of the eventual relation between the phase experimentally measured and the $\pi/2$ phase shift is still controversial⁷). The Kondo temperatures in the experiments on quantum dots are generally smaller than 1^0K and most importantly can be tuned via the gate voltage V_g . Therefore, the Kondo length scale is expected to be very large. Typically with a Fermi velocity $v_F = 5 \cdot 10^5 m/s$, ξ_K is of order 3 microns. Such low tunable Kondo temperature may therefore offer new opportunities to find evidence of this screening cloud.

Recently, we have proposed that persistent currents in a ring containing a quantum dot may offer a way to probe directly this large Kondo length scale.⁸ (See also Refs [9,10,11,12,13,14,15,16]). When the Kondo screening cloud becomes of order of the ring size or larger, we expect a crossover from a (large amplitude) saw tooth shape to a (small amplitude) sinusoidal shape. Unfortunately, persistent currents experiments are generally delicate and very sensitive to disorder. In or-

der to probe this fundamental length scale, it has been highly desirable to have some theoretical predictions based on conductance measurements which are more commonly used and better controlled.

Possible devices to probe the Kondo length scale might be a quantum dot embedded into or connected to a finite size geometry. Several geometries where some finite size effects due to the large Kondo length scale may occur have been proposed recently: possible geometries include a quantum dot connected to a box,^{17,18} a mesoscopic ring¹⁹ or a quantum dot embedded into short wires.^{20,21} The device we want to study in detail in this paper consists of a quantum dot embedded in two short wires (of length comparable to the Kondo length scale) which are then weakly coupled to some reservoirs. Such device is schematically depicted in Figure 1. One may wonder whether the conductance is sensitive to whether the Kondo cloud leaks into the reservoirs or is trapped inside the short leads. In the latter case, we may expect the conductance to be mainly dominated by the contacts between the reservoirs and the short leads. The answer is not so simple in the former case. Some partial results about this geometry have already been published elsewhere.²⁰ We have indeed studied a symmetric geometry, assuming the wires contain only one transverse channel, by means of perturbative calculations combined with a Fermi liquid approach when available. We have shown that when the bare Kondo temperature T_K^0 (defined by the Kondo temperature for infinite wires) is of the order or smaller than the energy level spacing in the wires, then the genuine Kondo temperature associated with the impurity can be very different from T_K^0 and strongly depends on the local density of states seen by the dot being on or off resonance. In this paper, we would like to provide a more detailed analysis of this geometry and discuss the generality of the predicted finite size effects. The plan of the paper is the following: in section 2, we present the tight binding model we want to study and give detailed derivations of these finite size effects using perturbation theory in the Kondo couplings. In section 3, we extend these results to wires which contain several transverse modes or channels. We note that the case of infinite length multi-channel wires has never been fully discussed to the best of our knowledge. In section 4, we show how these finite size effects affect quantitatively the transport properties through the quan-

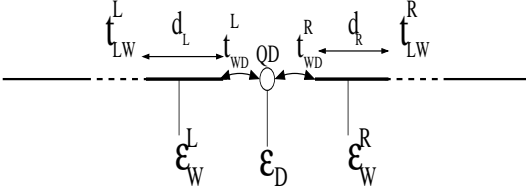


FIG. 1: Schematic representation of the device under consideration. ϵ_D and $\epsilon_W^{L/R}$ control respectively the dot and wires gate voltage.

tum dot. In section 5, we present complementary results valid at low temperature obtained with the Slave Boson Mean Field Theory (SBMFT). Finally in section 6, we discuss the main approximations made and the generality of our results. Three appendices with technical details are at the end of the paper.

II. FINITE SIZE EFFECTS IN A BOX GEOMETRY

A. Model Hamiltonian

In this section, we want to study the following system: a quantum dot embedded in a quantum wire which is in turn connected to external leads by weak tunnel junctions. We assume that a gate voltage can be applied to the dot and also to the quantum wires. A related device has been proposed recently by Thimm *et al.*¹⁷ where the quantum dot modeled by a standard Anderson Hamiltonian was coupled to all energy levels of a finite size box with the same (energy independent) tunneling amplitude. The energy level spacing was assumed constant and of $O(1/V)$ where V is the volume of the (3 dimensional) box. These two aspects differ considerably from the geometry studied here, since the electrons need to pass through the dot to contribute to the conductance. In fact, in the geometry studied in [17], the box is “side-coupled” to the dot whereas, here, the box embeds the dot. Moreover, the Non Crossing Approximation used in [17] might be questionable in such geometry where several new energy scales emerge compared to the usual Kondo model as was shown in [20]. We consider a one-dimensional tight-binding model which describes our device and has the Hamiltonian:

$$H = H_L + H_W + H_D + H_{LW} + H_{WD}, \quad (1)$$

where the subscripts L , W and D stand for leads, wires and dot respectively. Here:

$$\begin{aligned} H_L &= -t \left[\sum_{j=-\infty}^{-d_L-2} + \sum_{j=d_R+1}^{\infty} \right] (c_j^\dagger c_{j+1} + H.c.) \\ H_W &= -t \left[\sum_{j=-d_L}^{-2} + \sum_{j=1}^{d_R-1} \right] (c_j^\dagger c_{j+1} + H.c.) \\ &\quad + \epsilon_W^L \sum_{j=-d_L}^{-1} n_j + \epsilon_W^R \sum_{j=1}^{d_R} n_j \\ H_D &= \epsilon_D n_0 + U n_{0\uparrow} n_{0\downarrow} \end{aligned} \quad (2)$$

$$H_{LW} = -(t_{LW}^L c_{-d_L-1}^\dagger c_{-d_L} - t_{LW}^R c_{d_R}^\dagger c_{d_R+1} + H.c.)$$

$$H_{WD} = -(t_{WD}^L c_{-1}^\dagger c_0 + t_{WD}^R c_0^\dagger c_1 + H.c.)$$

Here $n_{j\sigma} \equiv c_{j\sigma}^\dagger c_{j\sigma}$ and $n_j \equiv n_{j\uparrow} + n_{j\downarrow}$. Note that t_{WD}^i and t_{LW}^i , with $i = L, R$ (this notation will be used throughout the paper), are the hopping amplitudes between the different sections of the geometry under consideration (see Figure 1). The spin indices have been omitted in order to lighten notations.

This Hamiltonian is a very simplified version of the geometry of interest in this paper. We assume that the quantum wires are in the ballistic regime and do not contain any other impurities (magnetic or not). We first consider the case of 1 channel where partial results have been reported elsewhere.²⁰ We will also discuss further a more realistic modeling of the quantum wires which typically contain 5 to 10 transverse channels³ at the end of this section. We ignore electron-electron interactions in the wires and leads, only keeping them in the dot. This point will be discussed in section VI.

We assume that the system is in the strong Coulomb blockade regime, so that $t_{WD} \ll -\epsilon_D, U + \epsilon_D$, where $\epsilon_D < 0$. Then we may eliminate the empty and doubly occupied states of the dot, so that $H_D + H_{WD} = H_K$ gets replaced by a Kondo interaction plus a potential scattering term:

$$\begin{aligned} H_K &= 2J(\kappa_L c_{-1}^\dagger + \kappa_R c_1^\dagger) \frac{\vec{\sigma}}{2} (\kappa_L c_{-1} + \kappa_R c_1) \cdot \vec{S} \\ &\quad + 2V(\alpha_L c_{-1}^\dagger + \alpha_R c_1^\dagger)(\alpha_L c_{-1} + \alpha_R c_1) \end{aligned} \quad (3)$$

with

$$J = ((t_{WD}^L)^2 + (t_{WD}^R)^2) \left[\frac{1}{-\epsilon_D} + \frac{1}{U + \epsilon_D} \right] \quad (4)$$

$$V = \frac{(t_{WD}^L)^2 + (t_{WD}^R)^2}{4} \left[\frac{1}{-\epsilon_D} - \frac{1}{U + \epsilon_D} \right] \quad (5)$$

and

$$\kappa_R = \frac{t_{WD}^R}{\sqrt{(t_{WD}^R)^2 + (t_{WD}^L)^2}} \quad \kappa_L = \frac{t_{WD}^L}{\sqrt{(t_{WD}^R)^2 + (t_{WD}^L)^2}} \quad (6)$$

Here \vec{S} is the spin operator for the quantum dot.

The Kondo effect can be understood as resulting from a renormalization of the Kondo coupling constant, J , to large values at low temperatures. Perturbation theory is infrared divergent but the temperature acts as an infrared cut-off yielding a finite result which is accurate if the temperature is sufficiently high ($T \gg T_K$). At low temperatures, a non-perturbative description is needed. This is provided by the local Fermi liquid description.²⁷ If we imagine that $J \gg t$, then a spin singlet forms in the groundstate from the impurity and an electron in a symmetric orbital on sites ± 1 . The anti-symmetric orbital still remains available to conduct current so the system is roughly equivalent to the $U = 0$ model and exhibits resonant conductance with the resonance tied to the Fermi surface.⁹

In the case of a closed ring, we showed earlier that the renormalization of the Kondo coupling is cut off, even at low

temperatures, by the ring circumference.⁸ In the present situation, this renormalization would be cut off by the finite length, $L = d_L + d_R$, of the quantum wires, if $t_{LW} = 0$. Essentially, if the Kondo cloud doesn't have enough space to form, then the growth of the Kondo coupling constant is cut off. The effective Kondo coupling at the length scale L becomes of $O(1)$ when $L \approx \xi_K$. Nevertheless, the situation is not so simple for small but finite t_{LW} . The growth of the Kondo coupling is no longer cut off by the finite size of the wire. Nonetheless, some noticeable finite size effects are expected to occur when L is reduced to a value of $O(\xi_K)$, which corresponds to the screening cloud beginning to leak into the leads.

B. Kondo temperature of the system

Before computing any thermodynamic or transport properties of the system, it is crucial to know the genuine Kondo temperature of our system, T_K , the main energy scale of the problem. In order to calculate T_K , we first diagonalize the Hamiltonian at $J = 0$, i.e. we diagonalize $H_0 \equiv H_L + H_W + H_{LW}$. Since the sites at $j < 0$ and $j > 0$ are completely decoupled in this limit, we can diagonalize the parts corresponding to the right and left leads separately. Let us first focus on the left part

only. If $t_{LW}^L = 0$, then the wave-functions and eigenvalues of the left part (corresponding to $-d_L \leq j \leq -1$) are:

$$\begin{aligned}\psi_L(j) &= (1/\sqrt{d_L}) \sin k_{L,n}j \\ k_{L,n} &= \pi n/(d_L + 1); \quad 1 \leq n \leq d_L \\ \varepsilon(k_{L,n}) &= -2t \cos k_{L,n} + \epsilon_W^L - \mu.\end{aligned}\quad (7)$$

For non-zero t_{LW}^L , the spectrum of H_0^L (the left part of H_0 is continuous). In order to study how the Kondo interaction renormalizes, we express c_{-1} in terms of the eigenstates, c_ϵ of $H_0^L - \mu N_L$:

$$c_{-1} = \int_{-2t-\mu}^{2t-\mu} d\epsilon f_L(\epsilon) c_{L,\epsilon}. \quad (8)$$

We have normalized the operators $c_{L\epsilon}$ so that $\{c_{L,\epsilon}^\dagger, c_{L,\epsilon'}\} = \delta(\epsilon - \epsilon')$. The left local density of states is defined by $\rho_L(\epsilon) = |f_L(\epsilon)|^2$ and is normalized according to $\int_{-2t-\mu}^{2t-\mu} d\epsilon \rho_L(\epsilon) = 1$. This local density of states can be easily computed exactly for our tight binding model. The calculation of $\rho_L(\epsilon)$ can be found in the appendix A. The final result, assuming $\gamma_L = t_{LW}^L/t \neq 0$ is

$$\rho_L(k) = \frac{1}{\pi t \sin^2 k_L (d_L + 1) - 2\gamma_L^2 \cos k \sin(k_L d_L) \sin(k_L (d_L + 1)) + \gamma_L^4 \sin^2(k_L d_L)} \gamma_L^2 \sin^2 k_L \sin k \quad (9)$$

where k_L is related to k by

$$-2t \cos k - \mu = -2t \cos k_L + \epsilon_W^L - \mu. \quad (10)$$

The fine structure and the properties of this local density of states has been studied in the appendix A. For small t_{LW}^L , this local density of states, $\rho_L(\epsilon) \equiv |f_L(\epsilon)|^2$, has sharp peaks at the energies $\epsilon_n = \epsilon_W - \mu - 2t \cos[k_{L,n}]$, where the momenta $k_{L,n}$ are solutions of the equation:

$$2k_L(d_L + 1) + \arctan \frac{\gamma_L \sin(k + k_L)}{1 - \gamma_L^2 \cos(k + k_L)} - \arctan \frac{\gamma_L \sin(k - k_L)}{1 - \gamma_L^2 \cos(k - k_L)} = 2\pi n, \quad (11)$$

with the constraint between k and k_L given by Eq. (10). For small γ_L , the solution of this equation is approximately

$$k_{L,n} \approx \pi n/(d_L + 1) + O(\gamma_L^2/d_L). \quad (12)$$

Plugging this value of $k_{L,n}$ in (10) provides the value of the gate voltage ϵ_W^L necessary to reach such a resonance. The separation between two consecutive peaks is approximately $\Delta_{L,n} \approx 2\pi \sin(k_{L,n})/d_L$. The width of these peaks can be also evaluated as

$$\delta_{L,n} = \frac{2(t_{LW}^L)^2 \sin^2(k_{L,n}) \sin(k)}{t(d_L + 1)}. \quad (13)$$

We can deduce that the ratio of width to separation for a peak defined by $k_{L,n}$ is of order:

$$\delta_{L,n}/\Delta_{L,n} \approx \frac{t_{LW}^2 \sin(k_{L,n}) \sin(k)}{t^2 \pi}. \quad (14)$$

We will assume that this quantity is $\ll 1$, a condition already encountered for $\gamma_L \approx 0.5$. Obviously, similar results are obtained for the right part of H_0 by changing $L \rightarrow R$.

The full Hamiltonian may be written in this basis as:

$$\begin{aligned}
H - \mu N_L - \mu N_R &= \int_{-2t-\mu}^{2t-\mu} d\epsilon \epsilon (c_{L,\epsilon}^\dagger c_{L,\epsilon} + c_{R,\epsilon}^\dagger c_{R,\epsilon}) \\
&+ \int d\epsilon d\epsilon' \left\{ f_L^*(\epsilon) f_L(\epsilon') \left(J_{LL} c_{L,\epsilon}^\dagger \frac{\vec{\sigma}}{2} \cdot \vec{S}_{c_{L,\epsilon'}} + V_{LL} c_{L,\epsilon}^\dagger c_{L,\epsilon} \right) + f_R^*(\epsilon) f_R(\epsilon') \left(J_{RR} c_{R,\epsilon}^\dagger \frac{\vec{\sigma}}{2} \cdot \vec{S}_{c_{R,\epsilon'}} + V_{RR} c_{R,\epsilon}^\dagger c_{R,\epsilon} \right) \right. \\
&\left. + \left(f_L^*(\epsilon) f_R(\epsilon') (J_{LR} c_{L,\epsilon}^\dagger \frac{\vec{\sigma}}{2} \cdot \vec{S}_{c_{R,\epsilon'}} + V_{LR}) c_{L,\epsilon}^\dagger c_{R,\epsilon'} + H.c. \right) \right\} \quad (15)
\end{aligned}$$

where we have defined $J_{LL} = 2\kappa_L^2 J$, $J_{RR} = 2\kappa_R^2 J$, $J_{LR} = 2\kappa_L \kappa_R J$. Similar definitions hold for the couplings V . It is worth noticing that these notations should not hide the fact that there is only one genuine Kondo coupling J and therefore only one Kondo temperature. Nevertheless, these notations are useful for transport properties as we be seen below.

Using the Hamiltonian in the form of Eq. (15), one can study how the Kondo couplings renormalize when the band-width is lowered from $\pm D_0$ (where D_0 is $O(t)$) to $\pm D$. At second order in the Kondo couplings, we obtain:

$$J_{ij} \rightarrow J_{ij} + \frac{1}{2} \sum_k J_{ik} J_{jk} \left[\int_{-D_0}^{-D} + \int_D^{D_0} \right] \frac{d\epsilon \rho_k(\epsilon)}{|\epsilon|}, \quad (16)$$

where $i, j, k = L$ or R . The renormalization of the Kondo couplings is quite different depending on how far we lower the cut off, D . If $D \gg \Delta_{i,n}$ ($i = L, R$), the integrals in Eq. (16) average over many peaks in the densities of states so their detailed structures become unimportant and we obtain the result for the usual Kondo model (see for example [25]). In particular, for a completely symmetric geometry, we recover the standard result $J \rightarrow J[1 + 2J\rho_0 \ln(D_0/D)]$ ($J = J_{LL} = J_{RR} = J_{LR}$).

On the other hand, for smaller D , $D \ll \Delta_{i,n}$, the renormalization of J in Eq. (16) becomes strongly dependent on the fine structure of the local densities of states and therefore of ϵ_W^L and ϵ_W^R . Let us analyze this in details in the next subsections.

1. Fully symmetric geometry

In order to simplify the picture, we first consider the completely symmetric case. In this subsection, most of the subscripts L and R have been suppressed. Let us first assume that ϵ_W is tuned to a resonance of the density of states of width δ_n . Then the integral in Eq. (16) gives a very small contribution as D is lowered from Δ_n down to δ_n so the renormalized Kondo coupling at the scale D , $J_{eff}(D)$, practically stops renormalizing over this energy range. Finally, when $D < \delta_n$, the density of states grows rapidly. To go further, we can approximate the local density of states (at the left or right part of the dot) by a sum of several Lorentzians of width δ_n :

$$\pi \rho_i(\epsilon) \approx \frac{2}{d_i} \sum_{n=1}^d \sin^2 k_{i,n} \frac{\delta_n}{(\epsilon - \epsilon_n)^2 + \delta_n^2}, \quad (17)$$

where $k_{i,n} = \pi n / (d_i + 1) + O(\gamma^2 / d_i)$ ($i = L = R$). This constitutes a quite good approximation when $\gamma^2 \ll 1$. For

example we have plotted in figure 2 the exact result and the approximate result for $\gamma = 0.5$. We see that both curve agree

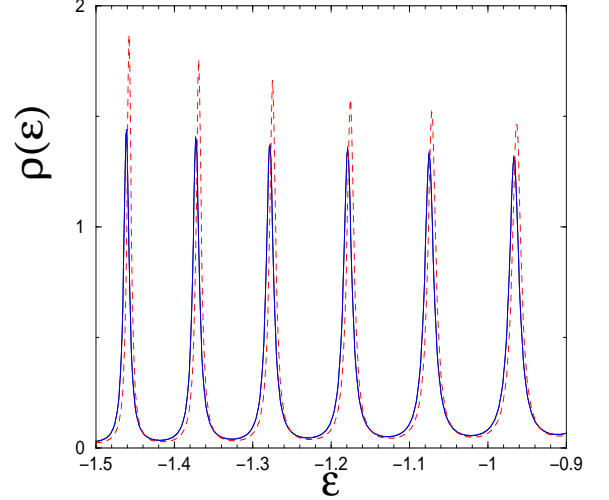


FIG. 2: The exact (plain blue curve) and the approximate (dashed red curve) local densities of states as a function of ϵ . We have taken $d = d_L = d_R = 49$ and $\gamma = 0.5$.

remarkably well even for $\gamma = 0.5$. They differ slightly in the height of the peaks and in the peak positions especially at the edges of the band.

We can express the result in terms of the change in $J_{eff}(D)$ as D is lowered from Δ_n around the resonance peak at $\epsilon = \epsilon_n$:

$$J_{eff}(D) \approx J_{eff}(\Delta_n) \left[1 + J_{eff}(\Delta_n) \frac{4 \sin^2(k_{i,n})}{\pi d \delta_n} \ln\left(\frac{\delta_n}{D}\right) \right], \quad (18)$$

where $d = d_L = d_R$. When ϵ_W is tuned exactly on resonance (i.e. $\epsilon_W = \epsilon_n$), the density of states appearing in this renormalization is enhanced by a factor of $(2t \sin^2 k_{i,n} / [d \sin k_n \delta_n]) \approx t^2 / [t_{LW}^2 \sin^2 k_n]$, k_n being related to $k_{i,n}$ by (10). This leads to a rapid growth of $J_{eff}(T)$.

On the other hand, if ϵ_W is off-resonance then the density of states is small, of order $(\delta_n / \Delta_n^2 d)$ so the growth of the Kondo coupling is very slow at all energies $D < \Delta_n$.

It is clear that this difference in the renormalization process between the two cases will strongly affect the Kondo temperature of the system. We define the Kondo temperature as the temperature where $J_{eff}(T)$ becomes of $O(1)$. When $J_{eff}(T)$ becomes large at $T \gg \Delta_n$ then T_K is related to the bare Kondo coupling and bandwidth as in the usual case (with no weak links): $T_K \approx T_K^0 \equiv D_0 e^{-1/2J\rho_0}$. Furthermore, in this case, T_K does not depend strongly on ϵ_W . We may characterize this case by $T_K^0 \gg \Delta_n$ or equivalently $\xi_K \ll L$. The screening cloud fits inside the quantum wires and the weak links do not modify the Kondo effect significantly.

On the other hand, suppose that $T_K^0 \ll \Delta_n$ implying that $J_{eff}(\Delta_n) \ll 1$. In this case T_K depends strongly on ϵ_W . If the system is tuned to a resonance then T_K will be slightly less than δ_n :

$$T_K^R \approx \delta_n \left(\frac{T_K^0}{D_0} \right)^{t_{LW}^2 \sin^2 k_n / t^2} = O(\delta_n), \quad (19)$$

On the other hand, if the system is off-resonance then $T_K \ll \delta_n$, the Kondo temperature reads

$$T_K^{NR} \approx \Delta_n \left(\frac{T_K^0}{D_0} \right)^{t^2 / (t_{LW}^2 \sin^2 k_{d,n})}. \quad (20)$$

In this equation the subscript NR stands for non resonant. In general, for small values of t_{LW}/t , we expect $T_K^{NR} \ll T_K^R$ (for experimental purposes, T_K^{NR} is almost 0). We have plotted the behavior of T_K vs. T_K^0 in Figure 3 for both ϵ_W on resonance and off resonance. This figure clearly illustrates the change of behavior when $T_K^0 \gg \Delta_n$ or $T_K^0 \ll \Delta_n$. The curves coincide for $T_K^0 \gg \Delta_n$ as expected. When $T_K^0 \sim \Delta_n$, the Kondo temperature begins to be sensitive to the fine structure in the local density of states which are signaled by the small oscillations of both T_K^R and T_K^{NR} (for the non resonant case, we have chosen the Fermi energy symmetrically between two resonant peaks). Note that there is a regime ($\Delta/2 < T < \Delta$) where $T_K^R > T_K^{NR}$. It corresponds to the situation where the integrals in (16) are dominated by two peaks for the off-resonance case and by one peak only for the on-resonance case. When $T_K^0 \ll \Delta_n$ the off resonance Kondo temperature T_K^{NR} drops sharply at $T_K^0 < \Delta_n$ to very small values ($\ll \delta_n$). On the other hand T_K^R also has a sharp drop at $T_K^0 < \Delta_n$ but then becomes almost flat and of order δ_n .

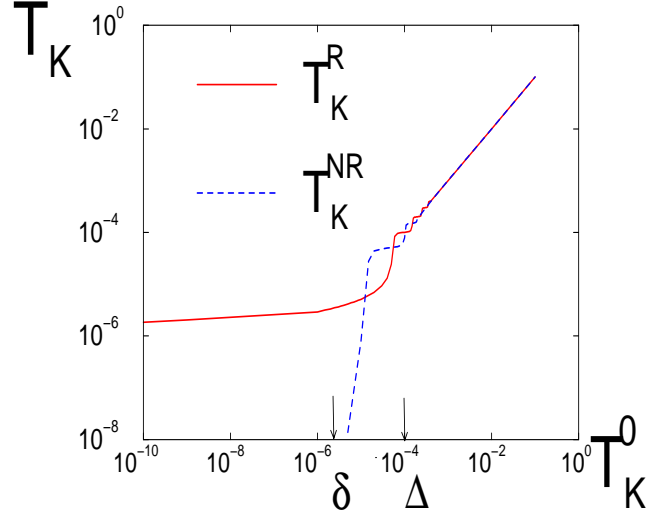


FIG. 3: The curves represent $T_K = f(T_K^0)$ in a log-log scale keeping the same values for Δ_n, δ_n for ϵ_W on resonance (plain curve which becomes almost flat at low $T_K^0 \ll \delta_n$), and ϵ_W off resonance (dashed curve which drops sharply at low T_K^0). Both curves coincide at $T_K^0 > \Delta_n$.

Since the Kondo temperature, the main energy scale, enters in the calculation of all most all the properties of the system, this strong difference of behavior between the on or off resonance case will affect dramatically all transport or thermodynamic quantities.

2. Non-symmetric geometry

If we consider now the general case of a non symmetric geometry, 3 different situations may occur by tuning the two gate voltages ϵ_W^L and ϵ_W^R : (i) they are both on resonances, (ii) both off resonances, or (iii) just one is on resonance. In case (i) or (ii), the physics will be very similar to what we discuss in the fully symmetric case. A natural way to define the Kondo temperature is to evaluate D such that the ratios between the second order corrections to the Kondo couplings and their bare values $J_{LL}^{(2)}/J_{LL}^{(0)}, J_{RR}^{(2)}/J_{RR}^{(0)}, J_{LR}^{(2)}/J_{LR}^{(0)}$ equals one. Since all the Kondo couplings are coupled together, we expect this to occur at the same value of $D = T_K$, the energy scale of the problem. Provided the local densities of states are of the same order of magnitude, the discussion in the previous section can be repeated. New features emerge for case (iii). Let us suppose that ϵ_W^L is tuned on resonance and ϵ_W^R off resonance. If T_K^0 is much larger than $\max(\Delta^L, \Delta^R)$, we

obviously recover the bulk situation with $T_K = T_K^0$. When T_K^0 is smaller than the level spacing, then T_K will depend on the fine structure of the densities of states. The RG equations (16) are then dominated by the resonance peak in the left lead. It means that the impurity is essentially screened in the left part of the device. Neglecting terms involving ρ_R in the flow (16), the Kondo temperature associated with this hybrid situation (we use the notation T_K^H for this hybrid case) can be evaluated as before as

$$T_K^H \approx \delta_n^L \left(\frac{T_K^0}{D_0} \right)^{2(t_{LW}^L)^2 \sin^2(k_n)/t^2} \approx (T_K^R)^2 / \delta_n. \quad (21)$$

We therefore also expect the Kondo temperature to be of order δ_n^L . Nevertheless, the strong asymmetry between the left and right part will affect transport properties.

III. EXTENSION TO THE MULTI-CHANNEL CASE

So far, we have modeled the short wires by a 1 dimensional tight binding model containing only 1 transverse channel. Nevertheless, the semiconducting wires contain in general 5 to 10 transverse modes. In this section, we discuss extensions of the previous results to take into account this multi-channel situation. Before considering the general case of finite length wires, we report for completeness on the more standard case of infinite wires connected to a quantum dot.

A. Case of infinite wires

1. Tight binding formulation

This situation can be easily taken into account by introducing in our tight binding Hamiltonian formulation a channel index (or band index) $\alpha = 1, \dots, N$ to the electron operators which labels the electronic eigenmodes in the transverse direction.

The tight binding Hamiltonian for infinite wires reads

$$\begin{aligned} H = & -t \left[\sum_{j=-\infty, \alpha}^{-2} + \sum_{j=1, \alpha}^{\infty} \right] (c_{j, \alpha}^\dagger c_{j+1, \alpha} + H.c.) \\ & - \sum_{\alpha} (t_{WD, \alpha}^L c_{-1, \alpha}^\dagger c_0 + t_{WD, \alpha}^R c_{1, \alpha}^\dagger c_0 + H.c.) \\ & - \sum_{\alpha, i} \mu_{\alpha} n_{i, \alpha} + \epsilon_D n_0 + U n_{0, \uparrow} n_{0, \downarrow} \end{aligned} \quad (22)$$

Note that the spin indices have been omitted. It is straight forward to extend the analysis developed in the previous section. After a Schrieffer-Wolff transformation, the Kondo interaction reads:

$$\begin{aligned} H_K = & \sum_{\alpha, \beta=1}^N \left[J_{\alpha, \beta}^{LL} c_{-1, \alpha}^\dagger \frac{\vec{\sigma}}{2} \cdot \vec{S}_{c_{-1, \beta}} + J_{\alpha, \beta}^{RR} c_{1, \alpha}^\dagger \frac{\vec{\sigma}}{2} \cdot \vec{S}_{c_{-1, \beta}} \right] \\ & + \sum_{\alpha, \beta=1}^N \left[J_{\alpha, \beta}^{LR} c_{-1, \alpha}^\dagger \frac{\vec{\sigma}}{2} \cdot \vec{S}_{c_{1, \beta}} + H.c. \right]. \end{aligned} \quad (23)$$

with

$$J_{\alpha, \beta}^{ij} = 2t_{WD, \alpha}^i t_{WD, \beta}^j / \tilde{\epsilon}_D \quad (24)$$

with $\tilde{\epsilon}_D = \left(\frac{1}{-\epsilon_D} + \frac{1}{-\epsilon_D + U} \right)$. In this section, we neglect the direct scattering terms since they turn out to be unimportant for our discussion. In order to study the renormalization of this set of Kondo couplings, it may be more convenient to momentarily suppress the distinction between left and right lead and to directly work with $2N$ channels. This can be done by $c_{-j, \alpha} \rightarrow c_{j, \alpha+N}$, $J_{\alpha, \beta}^{LL} \rightarrow J_{\alpha+N, \beta+N}$ and $J_{\alpha, \beta}^{LR} \rightarrow J_{\alpha+N, \beta}$. We will switch between these two notations throughout this section. With these notations, the RG equations take a simple form

$$J_{\alpha\gamma} \rightarrow J_{\alpha\gamma} + J_{\alpha\gamma} \sum_{\beta} J_{\beta\beta} \int d\epsilon \frac{\rho_{\beta}(\epsilon)}{|\epsilon|}, \quad (25)$$

where we have introduced $\rho_{\beta}(\epsilon)$ the local density of states seen by the dot in the channel $1 \leq \beta \leq 2N$. Note that the equation (25) follows from the fact the Kondo coupling $J_{\alpha\beta}$ can be written as a product of a term related to channel α with a term related to channel β . This product form is preserved under RG at least to lowest order. One may also introduce the dimensionless Kondo couplings constants

$$\lambda_{\alpha, \beta} = \sqrt{\rho_{\alpha} \rho_{\beta}} J_{\alpha, \beta}. \quad (26)$$

Since we consider infinite wires, it seems reasonable to assume that the densities of states are constant ($\rho_{\alpha} = \sin(k_{F, \alpha})/\pi t$ in our tight binding model) in each channels such that the RG equations can be further simplified to

$$\frac{d\Lambda}{d \log l} = \Lambda^2 + O(\Lambda^3), \quad (27)$$

where $\Lambda = (\lambda_{\alpha, \beta})$ is a matrix of Kondo couplings. As usual the RG equations make sense provided $\lambda_{\alpha, \beta}^{(0)} \ll 1$. All the couplings constant are driven to the strong coupling regime. Nevertheless, there is only one scale in the problem. This can be seen by noticing that the matrix Λ^0 (which defines the bare values of the Kondo couplings) has only one non zero eigenvalue ($= \text{Tr} \Lambda^0$). This is directly related to the fact that only one ‘‘effective’’ channel couples at the boundary to the impurity. Therefore, the Kondo temperature can be defined by:

$$T_K^0 = D \exp \left[-1/\text{Tr}(\Lambda^{(0)}) \right]. \quad (28)$$

At $T \ll T_K^0$, the impurity is screened by this ‘‘effective’’ channel. It is straightforward to extend the analysis of Ng and Lee²³ (which relies on the Langreth description of the low temperature Anderson model²⁴) in order to prove that the conductance through a quantum dot *symmetrically* connected to two identical leads (containing several channels) reaches the unitary limit $2e^2/h$. In the more general case corresponding to two leads non identically connected to the dot, the $T = 0$

conductance in the Kondo regime reads

$$G = \frac{2e^2}{h} \frac{\sum_{\alpha,\beta=1}^N 4\Gamma_\alpha^L(\epsilon_F)\Gamma_\beta^R(\epsilon_F)}{\left[\sum_{\alpha=1}^N (\Gamma_\alpha^L(\epsilon_F) + \Gamma_\alpha^R(\epsilon_F))\right]^2}, \quad (29)$$

with $\Gamma_\alpha^L(\epsilon) = (t_{WD,\alpha}^L)^2 \sin(k_{F,\alpha})/t$.

2. Continuum limit formulation

It seems also interesting to look at this multichannel case in the continuum limit. We have seen and concluded in the previous subsection that one ‘‘effective’’ channel couples at the boundary to the impurity. One may therefore wonder whether we can reduce the multi-channel problem to a single channel one. In order to formulate this model in the continuum limit, we may linearize the spectrum of the left/right leads around the $2N$ different Fermi points as:

$$c_\alpha^{L/R}(x) = c_\alpha(\pm x) = e^{-ik_{F,\alpha}x} \psi_{R,\alpha}^{L/R}(x) + e^{ik_{F,\alpha}x} \psi_{L,\alpha}^{L/R}(x) \quad (30)$$

$\forall x > 0$ and where $\psi_{L,\alpha}^{L/R}$ represents a left moving electron in the left or right lead. Instead of working with left and right movers living on a semi infinite line we can work with left movers only on the infinite line using the fact that we have perfectly reflecting boundary conditions. The linearized Hamiltonian reads:

$$H_{lin} = \int_{-\infty}^{+\infty} dx \left(\sum_{\alpha=1}^N \sum_{i=L,R} \frac{v_\alpha^F}{2\pi} (\psi_{L,\alpha}^i)^\dagger(x) i \partial_x \psi_{L,\alpha}^i(x) + \frac{\delta(x)}{2\pi} \sum_{\alpha,i} [t_\alpha^i c_d^\dagger \psi_{L,\alpha}^i(x) + H.c.] \right) + H_D, \quad (31)$$

with $t_\alpha^i = 2i \sin k_{F,\alpha} t_{WD,\alpha}^i$, $v_\alpha^F = 2t \sin(k_{F,\alpha})$ and i labels the left and right side of the dot. Since the impurity couples only to one linear combination of operators $\psi_{L,\alpha}^i(0)$, it may be tempting to introduce a new field basis defined by a unitary transformation U^i to the field ψ_α^i defined by

$$\eta_1^i = \sum_\alpha u_{1,\alpha} \psi_\alpha^i \quad \text{with} \quad u_{1,\gamma} = \frac{t_\gamma^i}{\sqrt{\sum_\alpha |t_\alpha^i|^2}}. \quad (32)$$

The other set of operators η_α^i with $\alpha > 1$ can be built in such a way for the matrix $U = (u)_{\alpha,\beta}$ to be unitary by the Schmidt orthonormalization process. Nevertheless, this unitary transformation leaves the kinetic part diagonal provided $v_\alpha^F = v^F \forall \alpha$. If this condition is met, the Anderson impurity model reduces in this new basis only to one effective channel. A similar conclusion was recently reached independently by Cho et al.²² considering several independent leads (containing one transverse channel). Since at low temperature, transport depends only on the Fermi level properties, the conductance through the dot will be dominated by one effective channel. In

particular, for a symmetric geometry, we recover that the conductance may reach at most the value $2e^2/h$ corresponding to the unitary limit. Nevertheless, for several transverse modes in a wire the condition $v_\alpha^F = v^F$ is most likely not satisfied and the introduction of the unitary transformation U may be not very helpful since it does not leave the kinetic energy diagonal. (One can still argue that the difference between Fermi velocities is usually irrelevant in 1D systems and the conclusions obtained above should hold.) Therefore, when the Fermi velocities are different, we need to perform some RG analysis analogous to what was developed in the previous section. In this formulation, the Kondo Hamiltonian reads:

$$H_K = \sum_{\alpha,\beta=1}^{2N} \sqrt{v_\alpha^F v_\beta^F} \lambda_{\alpha,\beta} \psi_\alpha^\dagger \frac{\vec{\sigma}}{2} \cdot S \psi_\beta \quad (33)$$

where $\lambda_{\alpha,\beta}$ has been defined in (26). Note that we have used the compact notation with $2N$ channels in order to avoid the distinction between left and right wires. Starting from Eq. (33), one can obtain in a similar manner the RG equations given in Eq. (27)

B. Case of finite size wires

In this section, we extend our previous results to take into account the fact that the wires are now finite and contain several channels. A possible Hamiltonian which extends Eq. (1) and describes this situation reads

$$H = H_L + H_W + H_D + H_{LW} + H_{WD} + H_G \quad (34)$$

with

$$H_L = -t \left[\sum_{j=-\infty,\alpha}^{-d_L-2} + \sum_{j=d_R+1,\alpha}^{\infty} \right] (c_{j,\alpha}^\dagger c_{j+1,\alpha} + h.c.) \quad (35)$$

$$H_W = -t \left[\sum_{j=-d_L,\alpha}^{-2} + \sum_{j=1,\alpha}^{d_R-1} \right] (c_{j,\alpha}^\dagger c_{j+1,\alpha} + h.c.) + \epsilon_W^L \sum_{j=-d_L,\alpha}^{-1} n_{j,\alpha} + \epsilon_W^R \sum_{j=1,\alpha}^{d_R} n_{j,\alpha} \quad (36)$$

$$H_{LW} = - \sum_{\alpha,\beta} (t_{LW,\alpha\beta}^L c_{-d_L-1,\alpha}^\dagger c_{-d_L,\beta} - t_{LW,\alpha\beta}^R c_{d_R,\alpha}^\dagger c_{d_R+1,\beta} + H.c.) \quad (37)$$

$$H_{WD} = - \sum_\alpha (t_{WD,\alpha}^L c_{-1,\alpha}^\dagger c_0 + t_{WD,\alpha}^R c_0^\dagger c_{1,\alpha} + H.c.) \quad (38)$$

$$H_G = - \sum_{\alpha,i} \mu_\alpha n_{i,\alpha}. \quad (39)$$

H_D is the dot Hamiltonian and remains unchanged compared to 1. Note that the tunneling amplitudes between the wires and the leads mix together the channels. Allowing channel mixing will not change much our discussion as we will see

further. The different bands have dispersion relations

$$\begin{aligned}\varepsilon_\alpha(k) &= -2t \cos k - \mu_\alpha \\ &= -2t \cos k_L + \epsilon_W^L - \mu_\alpha \\ &= -2t \cos k_R + \epsilon_W^R - \mu_\alpha.\end{aligned}\quad (40)$$

1. Without channel mixing

Before treating the general case of a matrix of tunneling amplitudes between the wires and the leads, we first consider in this subsection the simpler case where the matrices $t_{WL}^{L/R}$ are diagonal in the channel index. Such an approximation is valid when the wires and the leads are geometrically similar (i.e. with the same number of transverse modes) and the tunneling barrier separating them has no dependence on the transverse direction.

The fact that $t_{LW,\alpha} \neq t$ does not modify much the discussion made in section III A. A Schrieffer-Wolff transformation leads to the same Kondo Hamiltonian given by Eq. (23). The main difference is that the local density of states seen by the quantum dot acquires some non trivial energy dependence. Therefore, the RG equations corresponding to Eq. (25) are still valid. The density $\rho_\alpha(\epsilon)$ generalizes Eq. (9) with $\gamma_L \rightarrow \gamma_\alpha = t_{WL,\alpha}/t$, $k_L \rightarrow k_\alpha$, $\mu \rightarrow \mu_\alpha$ and corresponds to the LDOS in channel $1 \leq \alpha \leq 2N$ (within this compact notation $t_{WL,\gamma}^R = t_{WL,\gamma}$, $t_{WL,\gamma}^L = t_{WL,\gamma+N} \forall \gamma \in [1, N]$). Note that there is still only one scale in the problem, the Kondo temperature $T_K = D \exp[-/Tr(\Lambda(0))]$, which depends on the local density of states seen by the impurity, more exactly on the total tunneling amplitude $\Gamma(\epsilon) = \pi \sum_\alpha t_{WD,\alpha}^2 \rho_\alpha(\epsilon)$ (see Eq. (26)).

The properties of ρ_α are therefore similar to those of $\rho_L(\epsilon)$ studied in section II B. Let us for example analyze the total left tunneling amplitude seen by the quantum dot defined by $\Gamma_L(\epsilon) = \pi \sum_{\alpha=N+1}^N t_{WD,\alpha}^2 \rho_\alpha(\epsilon)$. Since the μ_α are different,

In this basis, the Kondo Hamiltonian reads:

$$\begin{aligned}H_K &= \int \int d\epsilon d\epsilon' \sum_{\alpha,be} \sum_{\gamma,\delta} \left[f_{L,\alpha,\gamma}^* f_{L,\alpha,\gamma} J_{\alpha,\beta}^{LL} c_{L,\gamma}^\dagger(\epsilon) \frac{\vec{\sigma}}{2} \cdot \vec{S}_{L,\delta}^\dagger(\epsilon') + f_{R,\alpha,\gamma}^* f_{R,\alpha,\gamma} J_{\alpha,\beta}^{RR} c_{R,\gamma}^\dagger(\epsilon) \frac{\vec{\sigma}}{2} \cdot \vec{S}_{R,\delta}(\epsilon') \right] \\ &+ \left[f_{L,\alpha,\gamma}^* f_{R,\alpha,\gamma} J_{\alpha,\beta}^{LR} c_{L,\gamma}^\dagger(\epsilon) \frac{\vec{\sigma}}{2} \cdot \vec{S}_{R,\delta}(\epsilon') + H.c \right],\end{aligned}\quad (42)$$

where the couplings $J_{\alpha,\beta}^{i,j}$ have been defined in Eq. (24). One may define new tunneling amplitudes $v_\gamma^i = \sum_\alpha f_{L,\alpha,\gamma} t_{WD,\alpha}^i$ (with $i = L, R$) and a new set of Kondo couplings:

$$\tilde{\lambda}_{\gamma,\delta}^{ij}(\epsilon, \epsilon') = (v_\gamma^i)^*(\epsilon) v_\delta^j(\epsilon') / \tilde{\epsilon}_D. \quad (43)$$

In this new basis, the problem takes a more familiar form with a $2N \times 2N$ matrix of Kondo couplings (if we again switch to the compact notation where no distinction between

the position of the peaks in the LDOS $\rho_{L,\alpha}$ are in general different. It implies that the *average* level spacing in the quantity $\Gamma_L(\epsilon)$ is now of order $\Delta_N^L = \pi v_F / Nd_L \approx \Delta_L / N$. Moreover the peaks have now different widths depending on $t_{WL,\alpha}^L$, μ_α and ϵ_W^L . The analysis developed in section II B extends straightforwardly: when T_K^0 becomes of order of or smaller than Δ_N^L , finite size effects appear in a completely similar way. It also implies from an experimental point of view that it is preferable to work with thin wires with a few transverse channels in order to reach the condition $T_K^0 < \Delta / N$. It is also worth mentioning that while in the 1 channel case, speaking about the ratios between Δ / T_K^0 or ξ_K^0 / d were equivalent, it is not the case here. We can no longer simply compare the Kondo screening cloud size to the length of the wire. Nevertheless, we can still define an effective length $d_{eff} = Nd$ which can be compared with ξ_K^0 .

2. With channel mixing

Suppose we now work with a more general model than (35) with a tunneling matrix $t_{WL,\alpha,\beta}^L$ between the left lead and the left wire (and the same in the right lead). We may express $c_{-1,\alpha}$ in terms of the eigenstates, $c_{L,\gamma}(\epsilon)$ of the left part of $H_L + H_W + H_{LW} + H_G$:

$$c_{-1,\alpha} = \int_{-2t-\mu}^{2t-\mu} d\epsilon \sum_\gamma f_{L,\alpha,\gamma}(\epsilon) c_{L,\gamma}(\epsilon). \quad (41)$$

The local density of states in the channel α at site -1 can be then defined by $\rho_\alpha(\epsilon) = \sum_\gamma |f_{L,\alpha,\gamma}(\epsilon)|^2$ and is normalized accordingly. This LDOS has a level spacing of order $\Delta \sim \hbar v_\alpha^F / d_L$ provided all the elements of the tunneling matrix are small compared to t . It implies that the resonance peak positions of $|f_{L,\alpha,\gamma}|$ are almost similar $\forall \gamma$ given by the ones of the isolated wire (up to a small shift of the order of the peak width which depends on the tunneling matrix).

left and right is made):

$$H_K = \int \int d\epsilon d\epsilon' \sum_{\gamma,\delta=1}^{2N} \tilde{\lambda}_{\gamma,\delta} c_\gamma^\dagger(\epsilon) \frac{\vec{\sigma}}{2} \cdot \vec{S}_\delta(\epsilon') \quad (44)$$

The RG equations have already been derived and read in this notation:

$$\tilde{\lambda}_{\gamma\delta} \rightarrow \tilde{\lambda}_{\gamma\delta} + \tilde{\lambda}_{\gamma\delta} \sum_\nu \int d\epsilon \frac{\tilde{\lambda}_{\nu\nu}(\epsilon)}{|\epsilon|}. \quad (45)$$

The coupling $\tilde{\lambda}_{\nu\nu}(\epsilon)$ has some non trivial energy dependence, since its bare value $\tilde{\lambda}_{\nu\nu}(\epsilon) \propto \sum_{\alpha} |f_{\alpha,\nu}(\epsilon)t_{WD,\alpha}|^2$. The average resonant peak spacing of $\sum_{\alpha} |f_{\alpha,\nu}|$ is $O(\hbar v_F/Nd)$ and the position of the peaks are almost independent of ν . Therefore, in order to calculate the Kondo temperature of the system, we need to compare T_K^0 to the energy scale $O(\hbar v_F/Nd) \equiv \Delta/N$ as in the non channel mixing case. To summarize, for weak tunneling amplitudes between wires and leads, the mixing of the channels just affects the fine structure of the local density of states seen by the quantum dot (i.e. the width of the peaks) but not the resonant peak positions (and therefore the level spacing) which is almost determined by the diagonalization of the isolated finite size wire. We note that this conclusion is quite general and should also be valid for the more realistic experimental situation of finite size wires

connected to $3D$ reservoirs.

IV. STUDY OF TRANSPORT PROPERTIES

We apply in this section the results obtained in the previous section in order to consider transport properties, in particular, the conductance through the device under consideration. As for thermodynamic properties, a perturbative calculation is instructive. We expect it to be valid at sufficiently high $T \gg T_K$ when the renormalized couplings are sufficiently small. The linear conductance (for $t_{LW}^i \neq 0$) at cubic order in J, V is given by:

$$G(T) = \frac{e^2}{\pi\hbar} \pi^2 \int d\epsilon \rho_L(\epsilon) \rho_R(\epsilon) [-dn_F/d\epsilon] \frac{3}{4} J_{LR}^2 [1 + J_{LL} I_L(\epsilon) + J_{RR} I_R(\epsilon)],$$

$$+ \frac{e^2}{\pi\hbar} 4\pi^2 V_{LR}^2 \int d\epsilon \rho_L(\epsilon) \rho_R(\epsilon) [-dn_F/d\epsilon] \quad (46)$$

with

$$I_L(\epsilon) = \int d\epsilon' PP \frac{\rho_L(\epsilon')}{(\epsilon' - \epsilon)} (1 - 2n_F(\epsilon')) \quad (47)$$

and a similar expression for I_R . PP stands for principal part and $n_F(\epsilon)$ is the Fermi distribution function at temperature T . These auxiliary functions leads to the usual logarithmic corrections. The derivation of this formula is sketched in the appendix B. We have not written the other contributions at cubic order since they do not involve logarithm divergences (and equal zero for particle-hole symmetry) and therefore do not renormalize in the infrared limit (see appendix B).

Notice too that the integral in the expression of $I_i(\epsilon)$ ($i = L, R$) depends on the local density of states $\rho_i(\epsilon)$.

Let us focus on the second order terms in J_{LR} and V_{LR} , and ignore, for the moment, the corrections of higher order. We must distinguish 3 regimes of temperature resulting simply from the fact that $(-dn_F/d\epsilon)$ has a peak with width of $O(T)$. If $T \gg \Delta_n^i$, then the integral in Eq. (46) averages over many peaks of $\rho_i(\epsilon)$ so that G is approximately independent of ϵ_W^i :

$$G \approx \frac{e^2}{\pi\hbar} (\pi\rho_0)^2 [3J_{LR}^2/4 + 4V_{LR}^2] \quad (48)$$

where $\rho_0 = \sin k_F/\pi t$ is the average local density of states.

When $\delta_n^i \ll T \ll \Delta_n^i$, the conductance depends strongly on the gate voltages ϵ_W^i . We then encounter three possibilities: i) both ϵ_W^i are tuned to a resonance peak, (ii) both are far from a resonance peak, (iii) only one of them, let us choose ϵ_W^L is tuned to a resonance peak. Let us detail these three cases:

(i) If both ϵ_W^i are tuned to a resonance peak such that $\epsilon_W^L = \mu + 2t \cos[k_{L,n}]$ and $\epsilon_W^R = \mu + 2t \cos[k_{L,m}]$, then the integral in Eq. (46) is dominated by the peaks located at $k_{L,n} \approx \pi n/(d_L + 1)$ and $k_{R,m} \approx \pi m/(d_R + 1)$ (notice that the integers n and m are in general different). In this regime of temperature, we can approximate $(-dn_F/d\epsilon) \approx 1/4T$. Moreover, we can neglect the other peaks except the resonant ones in the LDOS:

$$\pi\rho_L(\epsilon) \approx \frac{2 \sin^2(k_{L,n})}{d_L} \frac{\delta_n^L}{\epsilon^2 + (\delta_n^L)^2},$$

and we have a similar expression for $\pi\rho_R(\epsilon)$. Performing the integration we obtain for the on resonance conductance (subscript R):

$$G^R(T) \approx \frac{e^2}{\pi\hbar} \frac{(3J_{LR}^2/4 + 4V_{LR}^2)}{T d_L d_R} \frac{\pi \sin^2(k_{L,n}) \sin^2(k_{R,m})}{\delta_n^L + \delta_m^R}$$

$$\approx \frac{e^2}{\pi\hbar} (3J_{LR}^2/4 + 4V_{LR}^2) \frac{\pi t \sin^2(k_{L,n}) \sin^2(k_{R,m})}{2T \sin k [(t_{LW}^L)^2 d_R \sin^2(k_{L,n}) + (t_{LW}^R)^2 d_L \sin^2(k_{R,m})]} \quad (49)$$

For a completely symmetric geometry, this expression reads:

$$G^R(T) \approx \frac{e^2}{\pi\hbar} \frac{(3J_{LR}^2/4 + 4V_{LR}^2)}{2Tdt_{LW}^2} \pi t^2 \sin^2(k_{i,n}) \quad (50)$$

with $k_{i,n} = k_{L,n} = k_{R,m}$.

(ii) On the other hand, if both ϵ_W^i are far from a resonance peak (compared to T) then the LDOS is almost constant and may be approximated as $\pi\rho_L(\epsilon) \approx \frac{2\sin^2(k_{L,n})}{d_L} \frac{\delta_n^L}{\Delta_n^L}$. A similar expression for $\rho_R(\epsilon)$ can be written. Therefore the non resonant (subscript NR) conductance reads:

$$\begin{aligned} G^{NR}(T) &\approx \frac{e^2}{\pi\hbar} (3J_{LR}^2/4 + 4V_{LR}^2) \frac{\sin k_{L,n} \sin k_{R,m}}{\pi^2} \frac{\delta_n^L \delta_n^R}{(\Delta_n^L \Delta_n^R)^2} \\ G^{NR}(T) &\approx \frac{e^2}{\pi\hbar} (3J_{LR}^2/4 + 4V_{LR}^2) \frac{(t_{LW}^L)^2 (t_{LW}^R)^2 \sin^2 k_{L,n} \sin^2 k_{R,n} \sin^2 k}{\pi^4 t^6}. \end{aligned} \quad (51)$$

We also give the expression for the completely symmetric geometry

$$G^{NR}(T) \approx \frac{e^2}{\pi\hbar} (3J_{LR}^2/4 + 4V_{LR}^2) \frac{t_{LW}^4 \sin^4(k_{i,n}) \sin^2 k}{\pi^4 t^6}. \quad (52)$$

We immediately notice that $G^{NR}(T)/G^R(T) = O(t_{LW}^6/Tdt^5) \ll 1$.

(iii) Finally, if only ϵ_W^L is tuned on resonance, then the conductance associated to this hybrid (H) situation reads:

$$\begin{aligned} G^H(T) &\approx \frac{e^2}{\pi\hbar} (3J_{LR}^2/4 + 4V_{LR}^2) \frac{(t_{LW}^R)^2 \sin^2 k_{L,n} \sin^2 k_{R,n} \sin k}{2\pi T t^3 d_L} \\ &\approx \frac{e^2}{\pi\hbar} (3J_{LR}^2/4 + 4V_{LR}^2) \frac{\Delta_n^L \sin k_{L,n} \sin k_{R,n} \delta_n^R}{\Delta_n^R 4\pi T t^2}. \end{aligned} \quad (53)$$

The conductance G^H in this hybrid case is also small compared to G^R : $G^H(T)/G^R(T) = O(t_{LW}^4/Tdt^3) \ll 1$.

In the ultra-low temperature regime, $T \ll \delta_n^i$, one may evaluate the conductance in a similar way. by approximating $\pi\rho_i(\epsilon)$ by $2\sin^2(k_{i,n})/d_i\delta_n^i$. When ϵ_W^L and ϵ_W^R are both on resonance, we can approximate $\pi\rho_i(\epsilon)$ by $2\sin^2(k_{i,n})/d_i\delta_n^i$. The conductance then reads

$$G(T) \approx \frac{e^2}{\pi\hbar} \frac{(3J_{LR}^2/4 + 4V_{LR}^2)t^2}{(t_{LW}^L t_{LW}^R)^2 \sin^2 k} \quad (54)$$

The conductance is still given by Eq. (51) when ϵ_W^L and ϵ_W^R are both tuned off resonance for $T < \delta_n$. Finally, when only ϵ_W^L is tuned on resonance, the conductance reads:

$$G(T) \approx \frac{e^2}{\pi\hbar} ((3J_{LR}^2/4 + 4V_{LR}^2) \frac{\sin^2 k_{R,n}}{\pi^2} \frac{(t_{LW}^R)^2}{t^2 (t_{LW}^L)^2}) \quad (55)$$

We have used perturbation theory in order to evaluate the finite temperature conductance in all different situations. We have seen that the on-resonance conductance (where both wires are tuned on resonance) is far larger than the conductance in the other situations. This conclusion is valid only where perturbation theory applies. These approximate formulas certainly break down when they do not give $G\pi\hbar/e^2 \ll 1$, due to higher order corrections in J and V . So our approximate formulas will certainly break down before T is lowered to δ_n^i unless $J \ll (t_{LW}^i)^2/t$, a condition which might typically not be satisfied. When these formulas apply, we clearly

see that the conductance is much larger when ϵ_W^i are tuned on resonance.

However there is another, more interesting reason why these formulas can break down at low T , namely Kondo physics. The cubic correction in Eq. (46) contains a $\ln T$ term which essentially replaces J_{LR} by its renormalized value at temperature T , $J_{LR}^{eff}(T)$ following (16). We expect that this will remain true at higher orders.

Now consider the behavior of the conductance as a function of T and ϵ_W^i in the two cases. In the case $\xi_K \ll d_i$, we may calculate the conductance perturbatively in $J_{LR}^{eff}(T)$ at $T \gg T_K^0$ and using local Fermi liquid theory for $T \ll T_K^0$.²⁷ For $T \gg T_K^0$, we obtain Eq. (48), essentially independent of ϵ_W^i . On the other hand, for $T \ll T_K^0$, the conductance reduces to that of two reservoirs connecting each other by a contact whose conductance is

$$G_W = 2e^2/h (2t_{WL}^L t_{WL}^R)^2 / ((t_{WL}^L)^2 + (t_{WL}^R)^2)^2$$

(the low temperature conductance of the quantum dot in the Kondo regime). It corresponds to our original model with $U = 0$, $\epsilon_d = 0$, and some effective length $\tilde{d}_i \sim d_i$. (\tilde{d}_i can be somewhat reduced from d_i by an amount of order ξ_K). A general but less readable formula for the transmission associated to such non interacting geometry is given in appendix C. When $t_{WL}^L = t_{WL}^R$ and $\epsilon_W^L = \epsilon_W^R = \epsilon_W$, the quantum dot reaches the unitary limit and the conductance reduces to that

of an ideal wire of length $\tilde{L} = \tilde{d}_L + \tilde{d}_R$. The expression of

such conductance reads

$$G(T) = \frac{e^2}{\pi\hbar} \int 2t \sin k dk \frac{4(tt_{LW})^4 \sin^2 k_d \sin^2 k}{A^2 + B^2} \left[\frac{-dn_F}{d\epsilon}(k) \right] \quad (56)$$

with k_d defined by $\cos k_d = \cos k - \epsilon_W/2t$, and

$$\begin{aligned} A &= \sin[k_d(2\tilde{L} + 2)] - (\gamma_L^2 + \gamma_R^2) \cos k \sin[k_d(2\tilde{L} + 1)] + \gamma_L^2 \gamma_R^2 \cos 2k \sin[2k_d\tilde{L}] \\ B &= -(\gamma_L^2 + 2\gamma_R^2) \sin k \sin[k_d(2\tilde{L} + 1)] + \gamma_L^2 \gamma_R^2 \sin 2k \sin[2k_d\tilde{L}] \end{aligned}$$

As T is lowered below Δ_n^i the conductance for a symmetrically connected quantum dot develops peaks with spacing of order $\Delta_n^i/2$ ($i = L, R$). This is the spacing of peaks in the density of states of a wire of length $L = d_L + d_R$, containing no quantum dot. It is half the spacing in the density of states of the model with $J = 0$, discussed above. Initially, as T is lowered below Δ_n , the peak width is of $O(T)$ and the peak height is of $O(2e^2\Delta_n t_{WL}^2/hTt^2)$. As T is lowered below δ_n the peak width becomes of $O(\delta_n)$ and the peak height becomes of $O(2e^2/h)$. For a non symmetrically connected quantum dot ($t_{WL}^L \neq t_{WL}^R$), the halving of the period occurs when the Kondo quantum dot has a large enough conductance. In particular for two symmetric wires, we can prove using Eq. (A6) that the number of resonant peaks doubles when the condition

$$|R_D| < \frac{2|R_{LW}|}{1 + |R_{LW}|^2} \quad (57)$$

is satisfied. In this equation, we have defined $R_D = (t_{LW}^L)^2 - (t_{LW}^R)^2 / ((t_{LW}^L)^2 + (t_{LW}^R)^2)$, the reflection probability of the dot at low temperature and R_{LW} the reflection probability of the left or right weak link.

On the other hand, when $\xi_K \gg d_L, d_R$, the dependence of conductance on T and ϵ_W is very different. As T is lowered below Δ_n^i the on-resonance conductance starts to grow both because of the single-electron effects reflected in Eqs. (49) and (54) and, eventually, when $T \leq \delta_n$ because of the growth of $J_{eff}(T)$. However, off resonance the conductance stays small, given by Eq. (51) at least down to temperatures, $T \ll \delta_n$ of $O(T_K^{NR})$, given by Eq. (20). In the temperature regime $T_K^{NR} \ll T \ll \Delta_n$, the conductance has peaks with spacing Δ_n reflecting the fact that $J_{eff}(T)$ is small, off resonance. In Figure 4 we sketch the conductance versus ϵ_W in the two cases $T_K^0 \gg \Delta_n$ (dashed style) and $T_K^0 \ll \Delta_n$ (plain style) reflecting the halving of the period between the two curves. Note that we have used perturbation theory to plot the plain curve explaining why the amplitude is small. Nevertheless, at lower temperature, it is more difficult to calculate the on-resonance conductance both because of the breakdown of the perturbative result of Eq. (49), (54) due to single electron effects and because it appears considerably more difficult to extract unambiguous predictions from local Fermi liquid theory. Nonetheless, as we will check in the next section us-

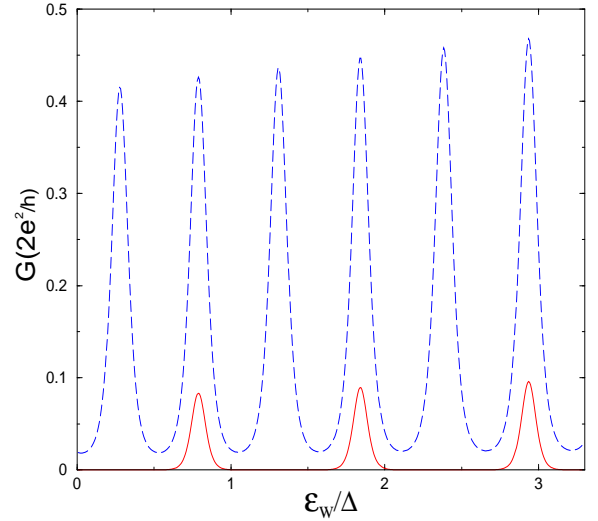


FIG. 4: Conductance in a symmetric geometry as a function of ϵ_W at fixed Δ_n, T and δ_n for both cases $\xi_K \gg d_L = d_R$ (plain style) and $\xi_K \ll d_L$ (dashed style). We have chosen $T \approx \Delta_n/10 \gg \delta_n \approx \Delta_n/100$. The curves have been represented on phase but in general they are expected to be shifted, the shift being difficult to determine.

ing slave boson mean field theory, it is very reasonable to expect a conductance of $O(1)$ on resonance at $T \leq \delta_n$ where $J_{eff}(T)$ is $O(1)$ on resonance. Off resonance we can show rigorously that the conductance remains small since $J_{eff}(T)$ remains small there and so do the single electron corrections to Eq. (51). The behavior of the conductance at very low $T \leq T_K^{NR}$ in the case $\xi_K \gg d$ will be also analyzed using the slave boson mean field theory.

In Figure 5, we have drawn schematically the conductance on resonance as a function of temperature for two different bare Kondo temperatures $T_{K,1}^0 \gg \Delta_n$ and $T_{K,2}^0 \ll \delta_n \ll \Delta_n$, using the perturbative formula given by Eq. (46) and the Fermi liquid picture valid for the first case only. For the first case, the conductance has a plateau which corresponds to the quantum dot being screened and the ϵ integral in Eq. (46) averaging over many peaks. The conductance reaches $2e^2/h$ only when $T \ll \delta_n$. Conversely, in the second case, the conductance remains small til $T \approx \delta$ where the Kondo

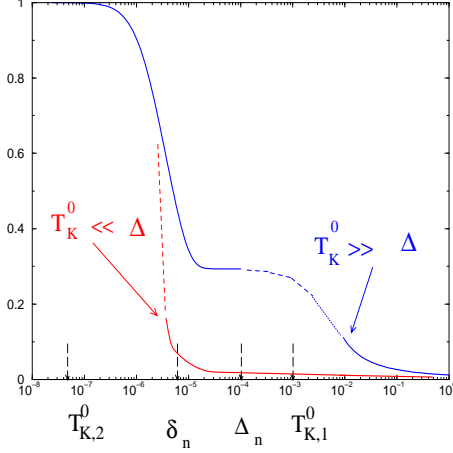


FIG. 5: Conductance as a function of temperature in a symmetric device (assuming both ϵ_{iW}^i is on resonance) for both cases $\Delta_n \ll T_{K,1}^0$ (right blue curve) and $\Delta_n \gg \delta_n \gg T_{K,2}^0$ (left red curve). The curves in plain style correspond to the perturbative calculations plus the Fermi liquid result for the first case only. We have schematically interpolated these curves (dotted lines) where neither the perturbative nor the Fermi liquid theory applies.

coupling becomes strongly renormalized (see Eq. (18)). We may expect a very abrupt increase of the conductance in this regime as schematically depicted in Fig 5. Notice that for this choice of $T_{K,2}^0$, the renormalized Kondo temperature $T_{K,2}^R$ is actually enhanced and of order δ_n . These different behaviors lead to different shapes of the curves.

V. SLAVE BOSON MEAN FIELD APPROXIMATION

We will use in this section the Slave Boson Mean Field Theory (SBMFT) in order to confirm qualitatively our analysis in the previous section.²⁶ This approximation seems to well describe qualitatively the behavior of the Kondo impurity at low temperature $T \ll T_K$ when the impurity is screened. It has recently been used by Hu *et al.*¹⁰ to calculate the persistent currents in a metallic ring containing a quantum dot and their results nicely confirm our perturbative and renormalization group calculations. This method assumes $U = \infty$ where the impurity operator can be written as $d_\sigma^\dagger = f_\sigma^\dagger b$, where the fermionic operator f_σ and the bosonic operator b describe the

singly occupied electron and holes states respectively. Furthermore, the constraint $b^\dagger b + \sum_\sigma f_\sigma^\dagger f_\sigma = 1$ has to be imposed. In the mean field approximation, the boson operator is replaced by a c-number b_0 . The constraint is implemented by using the Lagrange parameter λ_0 . Therefore, in the mean field approximation, the Hamiltonian is the same as in (1) with the following changes

$$\begin{aligned} H_{WD} &= -b_0(t_{WD}^L c_{-1}^\dagger f + t_{WD}^R f_0^\dagger c_1 + H.c.) \quad (58) \\ H_D &= \epsilon_0 f^\dagger f + \lambda_0 (b_0^2 - 1), \end{aligned}$$

where we have defined $\epsilon_0 = \epsilon_D + \lambda_0$.

Within this approximation, the Hamiltonian reduces to a non interacting system. The values of λ_0 and b_0 can be determined self-consistently by minimizing the free energy of the system defined by $F_{MF} = -\frac{1}{\beta} \log Z + \lambda_0 (b_0^2 - 1)$ with

$$Z = \prod_k (1 + e^{-\beta(\epsilon_k - E_F)})^2 \quad (59)$$

with E_F the Fermi energy and ϵ_k the energy eigenvalues of the mean field Hamiltonian. Once b_0 and λ_0 are found, we may directly apply the Landauer formula to find the conductance at finite temperature of the whole system. This is made possible because the mean field Hamiltonian is a non interacting one. We also want to emphasize that it is crucial to incorporate from the beginning the reservoirs when calculating the numerical parameters (here b_0 and λ_0) characterizing the quantum dot, especially in the limit $d_L, d_R \ll \xi_K^0$. Note that in [17], the quantum dot retarded Green function was calculated numerically using the non-crossing approximation without incorporating the reservoirs (i.e. by taking $t_{WL}^i = 0$). This might be a crude approximation especially in the limit $d \ll \xi_K^0$.

The mean field free energy is conveniently expressed as:

$$F_{MF} = -\frac{2}{\pi} \int_{-D_0}^{D_0} d\epsilon n_F(\epsilon) \text{Im}(\ln G_f^r(\epsilon)) + \lambda_0 (b_0^2 - 1), \quad (60)$$

where $n_F(\epsilon) = 1/[1 + \exp(\beta(\epsilon - \mu))]$ and G_f^r is the retarded Green function at the impurity. Using the approximate expression (17) for the left and right local density of states, the free energy reads:

$$F_{MF} = \frac{2}{\pi} \int_{-D_0}^{D_0} d\epsilon n_F(\epsilon) \arctan \left(\frac{\sum_{i=L,R} b_0^2 (t_{WD}^i)^2 \Sigma_1^i(\epsilon)}{\epsilon - \epsilon_0 - \sum_i b_0^2 (t_{WD}^i)^2 \Sigma_2^i(\epsilon)} \right) + \lambda_0 (b_0^2 - 1), \quad (61)$$

where

$$\Sigma_1^i = \frac{2}{d_i} \sum_{n=1}^{d_i} \sin^2 k_{i,n} \frac{\delta_{i,n}}{(\epsilon - \epsilon_{i,n})^2 + \delta_{i,n}^2} \quad (62)$$

$$\Sigma_2^i = \frac{2}{d_i} \sum_{n=1}^{d_i} \sin^2 k_{i,n} \frac{(\epsilon - \epsilon_{i,n})}{(\epsilon - \epsilon_{i,n})^2 + \delta_{i,n}^2}. \quad (63)$$

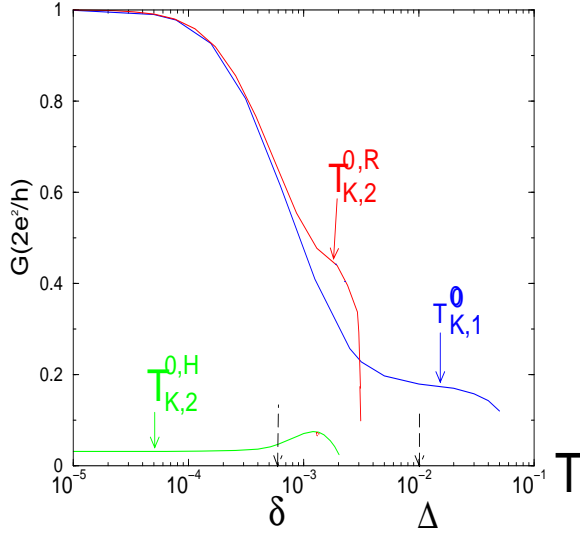


FIG. 6: Conductance from SBMFT as a function of temperature for two bare Kondo temperatures $T_{K,1}^0 \approx 3.6\Delta$ and $T_{K,2}^0 \approx \Delta/10$. For the latter case, we have considered the 3 cases depending on ϵ_{iW}^i being both on resonance (corresponding to $T_{K,2}^{0,R}$), both off resonance (corresponding to $T_{K,2}^{0,NR}$) or the hybrid situation (corresponding to $T_{K,2}^{0,H}$). Here $\gamma = 0.3$. We have not plotted the off resonance case because T_K^{OR} seems very small in this case and our SBMFT has convergence difficulties.

By minimizing F_{MF} with respect to λ_0 and b_0 , we obtain a set of two self consistent equations which can be solved numerically by iteration. Since the formulation of the problem is non-interacting, the conductance can be expressed using the Landauer formula

$$G = \frac{2e^2}{h} \int d\epsilon \left(\frac{-dn_F}{d\epsilon} \right) T(\epsilon), \quad (64)$$

where $T(\epsilon)$ is the total transmission probability through the non interactive device in the SBMFT, the quantum dot is modeled by a simple resonant level with $U = 0$, $t_{WL}^i \rightarrow b_0 t_{WL}^i$ and $\epsilon_0 = \epsilon_D + \lambda_0$. The expression for T is given in the appendix B by the Eq. (C1).

A. Analysis of the symmetric geometry

As in the previous section, we have fixed d (therefore the level spacing Δ) and considered different bare Kondo temperatures corresponding to both limits $T_K^0 \ll \Delta$ and $T_K^0 \gg \Delta$, where Δ is the level spacing at the Fermi energy inside the wires. In the following, we assume that $t_{WD}^L = t_{WD}^R$, $t_{LW}^L = t_{LW}^R = \gamma t$ and $d_L = d_R = d$.

We have plotted the conductance as a function of temperature for two different bare Kondo temperatures $T_{K,1}^0 \approx 3.6\Delta$ and $T_{K,2}^0 \approx \Delta/10$ for $\gamma = 0.3$ (Figure 6) and $\gamma = 0.5$ (Figure 7). For $T_{K,2}^0$, we have considered three cases: both left and right wires are on resonance, both wires are off resonance and finally only one of them is on resonance. Such a distinction

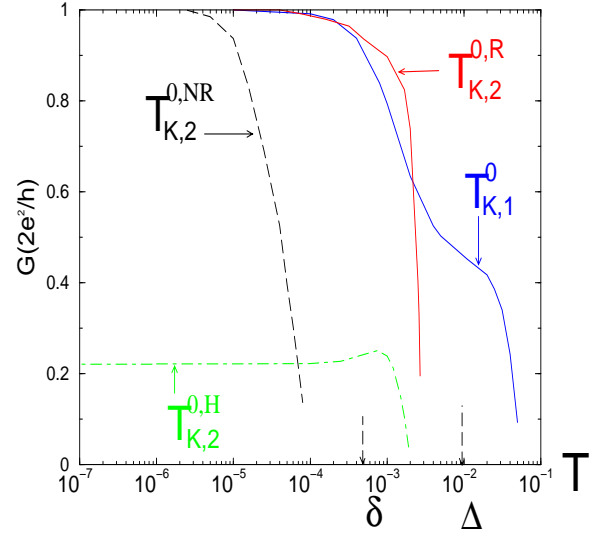


FIG. 7: Same as Fig. 6 but with $\gamma = 0.5$. Note that here the 3 cases are plotted for $T_{K,2}^0 \approx \Delta/10$.

is not worth making for $T_{K,1}^0$ since all curves are very similar since the conductance does not depend of the fine peak structure of the LDOS. As previously emphasized, the SBMFT is a low temperature method complementary to our perturbation calculation. Therefore, we have stopped the curves at $T \approx T_K$ (not the bare one !) where the method failed or is meaningless. Moreover, some convergence problem may occur in this limit particularly for the case $T_K^0 \ll \Delta$ where the Kondo couplings get very strongly renormalized on a very small energy scale. Another more powerful numerical method like the Numerical Renormalization Group (NRG) carried out in Ref. [21] is required to estimate the conductance for the full crossover from low to high temperature.

Let us analyze the results now. In figure 6, the curve $T_{K,1}^0$ looks like the one predicted in Figure 5. It has a plateau around $T = \Delta$ separating the low temperature where the unitary limit is reached from the high temperature perturbative regime (almost not shown here). The curves for $T_{K,2}^{0,R}$ is different and does not exhibit such an intermediate plateau. On the other hand, when the temperature is increased, it suddenly shoots down abruptly at $T \approx T_{K,2}^R \approx 0.002 \approx 3\delta$. We quickly go from the low temperature regime to the high temperature regime where perturbation theory applies. Note that this sharp drop is also associated with the limit of convergence of the SBMFT in this situation (because the variational parameter b_0 becomes very small). This sharp change of behavior in the conductance was predicted by the perturbative analysis (see Figure 5) and is due to the strong renormalization of the Kondo coupling when the temperature reaches the order of the peak width. We have not plotted the conductance for the off resonance case where our result indicates a Kondo temperature $T_{K,2}^{NR} \approx 10^{-7}$ with an abrupt change too. The on resonance- off resonance curve exhibits a similar behavior as the on resonance one but its value at low temperature is very small due to the asymmetry. For $\gamma = 0.5$, we still observe an abrupt decrease of the conductance for $T_{k,2}^0$ in the three pos-

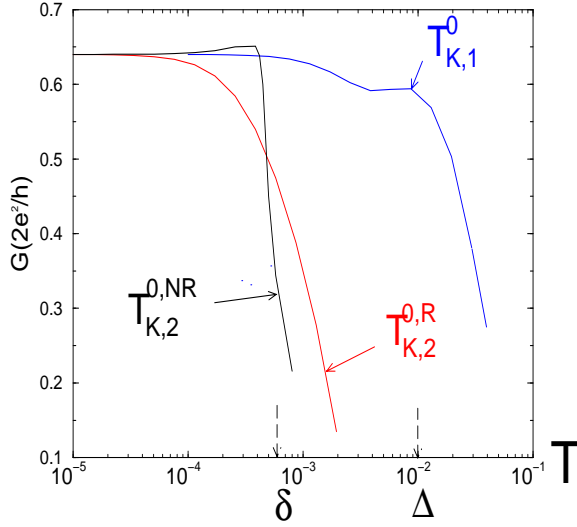


FIG. 8: Conductance as a function of temperature in a completely asymmetric geometry with only one short wire. We took $\gamma_L = 0.5$ and $\gamma_R = 1$. We have considered two bare Kondo temperatures $T_{K,1}^0 \approx 3.6\Delta$ and $T_{K,2}^0 \approx \Delta/10$.

sible situations. On the other hand, the difference of behavior between $T_{k,1}^0$ and $T_{k,2}^{0,R}$ has almost disappeared. In particular, the plateau around $T \approx \Delta$ for $T_{k,1}^0$ is now replaced by a shoulder. The only way to identify the situation $T_K^0 \ll \Delta$ relies on the dependence on the local densities of states being on or off resonance. For this purpose, we note that the behavior for the off resonance curve defined by the label $T_{K,2}^{0,NR}$ is very similar to the on resonance one defined by $T_{K,2}^{0,R}$, but translated toward lower temperature by roughly two order of magnitudes.

From this difference, we can immediately infer that the conductance function of the gate voltages $\epsilon_W^L = \epsilon_W^R$ exhibits a doubling of the period (compared to the case $T_K^0 \gg \Delta$) in the window $T_{K,2}^{NR} \ll T \ll T_{K,1}^0$. Instead of varying two gates voltage, we may imagine that we fix ϵ_W^L on resonance and study the conductance as a function of ϵ_W^R only (which is more convenient to realize experimentally). Suppose the temperature is also fixed at $T \approx \delta$ (see Figure 7). The curve corresponding to $T_K^0 \gg \Delta$ will exhibit resonance peaks of height $\approx 2e^2/h$ with the level spacing $\Delta/2$ as depicted in Figure 4. On the other hand, the curve corresponding to $T_K^0 \ll \Delta$ will exhibit a succession of large resonant peaks (of height $\approx 2e^2/h$) and small resonant peaks (of height $\approx 0.4e^2/h$), clearly different from the case $T_K^0 \gg \Delta$.

B. Analysis of the complete asymmetric geometry

One may wonder what happens if we connect only one short wire, the left one for example, to the quantum wire, an *a priori* easier situation to realize experimentally. In our model, it corresponds to $\gamma_R = 1$. In the figure 8, we have therefore plotted the conductance as a function of temperature for the two Kondo temperature $T_{K,1}^0 = 3.6\Delta \approx 0.36$ and

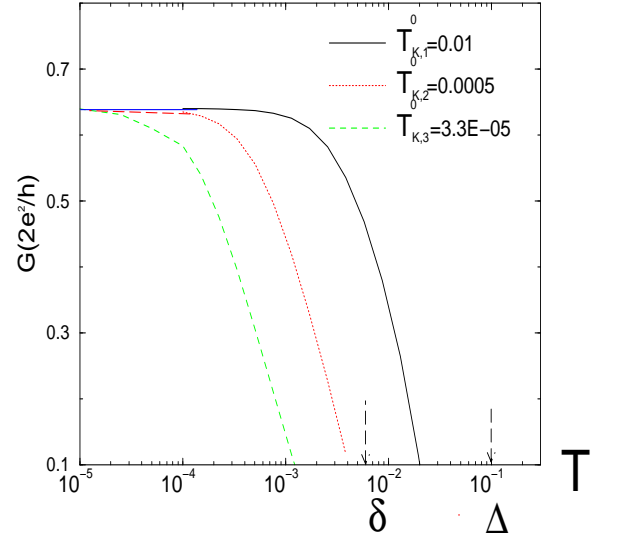


FIG. 9: Same as above. We have considered three bare Kondo temperatures (see the labels) which all correspond to $T_K^0 \ll \Delta$. Note that in this figure $\Delta \approx 0.1$ and $\delta \approx 0.006$.

$T_{K,2}^0 = \Delta/10 \approx 0.01$ (defined for infinite wires). Except for the shoulder around $T \approx \Delta$ for the curve $T_{K,1}^0$, the curves are very much alike. For the geometry with two wires, the best signature of the behavior $T_K^0 \ll \delta$ was the difference between the on- or off- resonance situations. Here this difference is not very dramatic (except for a sharper behavior for $T_{K,2}^{0,NR}$). The effective Kondo temperatures for both cases are around $T_{K,2}^0 = 0.001$ (slightly less for the off resonance case). It implies that the renormalization of the Kondo coupling is essentially dominated by the bulk part which does not contain any wire. In other words, the screening cloud builds mostly in the right lead. Nevertheless, it may not be always be so. Indeed, we have plotted in Figure 9, the on-resonance conductance for three different Kondo temperatures $T_{K,1}^0 = 0.1\Delta$, $T_{K,2}^0 = 0.005\Delta$ and finally $T_{K,3}^0 = 3.2 \cdot 10^{-4}\Delta$. The first Kondo temperature corresponds to a situation studied in Figure 8 where the screening is mainly dominated by the right lead. In other words, for such bare Kondo temperature, we do not expect much variation of the conductance with ϵ_W^L . The other two bare Kondo temperatures have been chosen such that $T_{k,2/3}^0 \ll \delta$. For such choice, we expect that the renormalization of the Kondo couplings will be dominated by the on resonance peak in the left LDOS. This corresponds, as mentioned in the previous section and exemplified here, to an enhancement of the Kondo temperature. From the conductance curves, one may infer a cross-over temperature which can interpreted as an effective Kondo temperature. One could approximately evaluate $T_{K,2} \approx 0.002 > T_{K,2}^0$ and $T_{K,2} \approx 0.0005 \gg T_{K,3}^0$. In such cases, one expect a strong dependence of the conductance with ϵ_W^L . Indeed, when ϵ_W^L is off resonance, the renormalization of the Kondo coupling will be again dominated by the right lead with an effective Kondo temperature $T_{K,3}^{OR} \approx T_{K,3}^0$. It implies that the conductance as a function of ϵ_W^L should exhibit peaks of spacing Δ_L for

the temperature range $T_{K,3}^{OR} \ll T \ll T_{K,3}^R$. To summarize the analysis of this completely asymmetric geometry, finite size effects associate with the formation of the Kondo screening cloud may occur only when the bare Kondo temperature is less than the resonance width. It implied very low Kondo temperatures which may not be within experimental reach.

VI. DISCUSSION AND CONCLUSION

In this paper, we have presented some detailed (analytical and numerical) calculations of a model describing a quantum dot embedded in two short wires which are connected to reservoirs. We have shown that finite size effects may occur when the Kondo temperature T_K^0 (for infinite wires) becomes of order of the level spacing inside the wires. The main consequence is that the genuine Kondo temperature of this system T_K may differ considerably from T_K^0 and furthermore becomes sensitive to the local fine structure of the local density of states seen by the quantum dot. The LDOS seen by the dot can be controlled by appropriate gate voltage $\epsilon_W^{L/R}$. It is also worth noting that experimentally it provides an extra parameter to control the Kondo temperature. This strong difference between T_K and T_K^0 has a signature in all transport and also thermodynamic properties as we have seen. An interesting smoking gun to detect these finite size effects is the halving of the period (see Figure 4) in the curve of conductance versus wire gate voltage $\epsilon_W^{R/L}$.

The symmetric version of the model analyzed in this paper has been investigated recently by Cornaglia and Balseiro²¹ using the numerical renormalization group. Their main conclusions is in agreement with ours (see also Ref. [20]). Nevertheless, on a more quantitative footing, we note that these authors found a non-monotonic behavior in some plots of the conductance as a function of temperature (particularly for the off resonance case). We have not found signatures of such behavior. This might be due to the breakdown of the SBMFT in the regime $T > T_K^{NR}$. We also note that a rather large width of the peaks in the LDOS was considered by Cornaglia and Balseiro (they typically take $\delta \sim T_K^0$) which prevents a distinction between the on-resonance case for $T_K^0 \ll \Delta$ and the standard case of infinite wires.

The analysis developed in the paper relies on some specific approximations we want to discuss.

First, we have assumed that all the conductors, the short wires included, are in a ballistic regime, or at least that the mean free path l_d is the largest length scale by far. If the mean free path l_d would be for example smaller than the length of the short wires, we would then need to compare the Kondo length scale ξ_K^0 with l_d and not with d the wire length.

We have also neglected the Coulomb interactions in the

wires. This is one of the most important approximation made in our treatment (which also makes the problem tractable). One open question is whether (and how) the genuine Kondo temperature of the system depends on the Coulomb interactions in the wires. The Coulomb interactions may also modify the transport properties through the whole system. For example, Coulomb blockade effects may appear in the conductance as a function of the wire gate voltage. Depending on the local density of states being on or off resonance, the conductance through the central quantum dot will be very large or instead very small (when finite size effects occur). Assuming Coulomb blockade phenomenon are important in the wires, such a system can be seen as a double quantum (large) dot connected by a weak/strong tunneling junction, a device which was studied in Ref. [29]. When the tunneling junction is weak it was found that the period of the peaks doubles compared to the strong tunneling limit. Indeed, for the small tunneling junction, the excitation spectrum consists of two independent spectra of the two dots/wires of size L whereas for a strong tunneling junction, the excitation spectrum is better described by the one of a single larger dot of size $2L$.²⁹ Therefore it may be tempting to argue that our prediction of the halving of the period in the conductance function of the wires gate voltage still occur when Coulomb interactions are incorporated. Nevertheless, a complete analysis incorporating consistently both the Coulomb interactions and the finite level spacing in the wires would be required and goes beyond the scope of the present paper. We hope to return to this more difficult but important problem in the future.

APPENDIX A: CALCULATION AND ANALYSIS OF THE LOCAL DENSITY OF STATES

In this appendix, we give the main steps of the derivation of the expression for the local density of states given by Eq. (9) in our tight binding model. We also study its main characteristics. In this appendix, we calculate the left LDOS, the right one is obtained by changing $L \rightarrow R$.

We write the wave function in site j with momentum k as

$$\begin{aligned}\psi(j) &= A \sin(k_L j) \text{ for } -d_L \leq j \leq -1 \\ \psi(j) &= B \sin(kj) + C \cos(kj) \text{ for } j \leq -d_L - 1\end{aligned}$$

where the wave vectors k and k_L are related through $-2t \cos k - \mu = -2t \cos k_L + \epsilon_W^L - \mu$.

B, C are related to A by writing the Schroedinger equations at sites $-d_L$ and $-d_L - 1$:

$$B = \frac{A \cos(kd_L) \sin(k_L(d_L + 1)) - \gamma_L^2 \cos(k(d_L + 1)) \sin(k_L d_L)}{\gamma_L \sin k} \quad (\text{A1})$$

$$C = \frac{A - \sin(kd_L) \sin(k_L(d_L + 1)) + \gamma_L^2 \sin(k(d_L + 1)) \sin(k_L d_L)}{\gamma_L \sin k}, \quad (\text{A2})$$

for $\gamma_L = t_{WL}^L/t \neq 0$. Moreover, suppose our system is embedded in a huge box of size $L \gg d$. Normalizing the wave functions to 1 in the box gives the relation $|B|^2 + |C|^2 = 2/L$. Therefore, A^2 reads

$$A^2 = \frac{2}{L} \frac{\gamma_L^2 \sin^2 k}{\sin^2(k_L(d_L + 1)) - 2\gamma_L^2 \cos k \sin(k_L(d_L + 1)) \sin(k_L d_L) + \gamma_L^4 \sin^2(k_L d_L)} \quad (\text{A3})$$

Notice that for $\gamma_L = 1$ and $\epsilon_W^L = 0$, we recover $A^2 = 2/L$. The local density of states is then given by $\rho_L(\epsilon) = A^2 \sin^2 k_L / (2t \sin k(\pi/L))$ with our normalization of the anti-commutation relations. We therefore obtain as a final expression the equation (9).

There is another way to derive such expression which is more convenient in order to study the properties of the local density of states. We consider the same geometry described in Figure 1. Instead of the quantum dot, we assume a direct tunneling of amplitude t' between the sites -1 and 1 . We also assume the geometry to be completely symmetric (i.e $d_L = d_R$, $\epsilon_W^L = \epsilon_W^R$ and $\gamma_L = \gamma_R$). For small t' the conductance can be calculated perturbatively in t' :

$$G = \frac{e^2}{\pi \hbar} 4(t')^2 \int d\epsilon (\pi \rho_L(\epsilon))^2 (-dn_F(\epsilon)/d\epsilon) + O(t'^4) \quad (\text{A4})$$

Since the system is non interacting, the conductance can be also computed exactly using the Landauer formula:

$$G = \frac{e^2}{\pi \hbar} \int d\epsilon |T_{tot}|^2(\epsilon) (-dn_F(\epsilon)/d\epsilon) \quad (\text{A5})$$

where $T_{tot}(\epsilon)$ is the total transmission amplitude through the system. For a wave number k , $T(k)$ reads:

$$T_{tot}(k) = \frac{T_{LW} T_{WL} T_0}{1 - 2R_0 R_{WL} e^{2ikd_L} + (R_{WL})^2 (R_0^2 - T_0^2) e^{2ikd}} \quad (\text{A6})$$

where R_{WL} is the reflection coefficient for the left and right weak link in sites $-d_L$ and d_R , T_{LW} is the transmission coefficient through the weak link for an electron coming from the lead, T_{WL} is the opposite and finally R_0, T_0 are the reflection and transmission coefficients through the central weak link. Since

$$T_0(k) = \frac{-2it' \sin k_L}{1 - t'^2 e^{2ik_L}} ; \quad R_0(k) = \frac{t'^2 - 1}{1 - t'^2 e^{2ik_L}} \quad (\text{A7})$$

the term in t'^2 is easily obtained by replacing in the denominator of Eq. (A6) $R_0(k)$ by -1 and $T_0(k)$ by 0 and keeping the first term in $T_0(k)$ in the numerator. Therefore, we can write

$$\pi \rho_L(k) = \sin k_L \left| \frac{T_{LW} T_{WL}}{1 - 2r_{wl} e^{2ikd_L + i\pi + i\theta_{WL}} + r_{WL}^2 e^{2ik(d) + 2i\theta_{WL}}} \right| = \sin k_L \frac{t_{lw} t_{wl}}{1 - 2r_{wl} \cos \alpha + r_{wl}^2} \quad (\text{A8})$$

where we have defined $R_{WL} = r_{wl} e^{i\theta_{WL}}$, $t_{wl} = |T_{WL}|$, $t_{lw} = |T_{LW}|$ and

$$\alpha = \pi + 2k_L d_L + \text{Arg}(R_{WL}) = 2k_L(d_L + 1) + \arctan \frac{\gamma_L^2 \sin(k + k_L)}{1 - \gamma_L^2 \cos(k + k_L)} - \arctan \frac{\gamma_L^2 \sin(k - k_L)}{1 - \gamma_L^2 \cos(k - k_L)}. \quad (\text{A9})$$

One can check explicitly that the expression in Eq. (A8) coincides with the one in Eq. (9). Fortunately, the equation in (A8) is much more compact and readable. One can for example immediately infer from (A9) that the positions of the peaks in the local density of states are given by the solutions of $\alpha = 2\pi n$ which gives the equation (11). The peak half-width $\delta_{L,n}$ can also be computed straightforwardly using the expressions

$$r_{wl} = \sqrt{\frac{(1 - \gamma_L^2 \cos(k - k_L))^2 + \gamma_L^4 \sin^2(k - k_L)}{(1 - \gamma_L^2 \cos(k + k_L))^2 + \gamma_L^4 \sin^2(k + k_L)}} ; \quad t_{lw} = \frac{2\gamma_L \sin k_L}{\sqrt{(1 - \gamma_L^2 \cos(k + k_L))^2 + \gamma_L^4 \sin^2(k + k_L)}}. \quad (\text{A10})$$

The expression for t_{wl} is obtained from t_{lw} by exchanging k with k_L . The height of a given peak labelled by n is given by

$$\pi \rho_L(k_n) = \sin k_{L,n} \frac{t_{lw} t_{wl}}{(1 - r_{wl})^2} \quad (\text{A11})$$

The width of the peak is obtained for

$$\delta \alpha \approx 2(d_L + 1) \delta k_L = (1 - r_{wl}) / \sqrt{r_{wl}}$$

which provides the expression (13) for the width (using $\delta \epsilon = 2 \sin k_L \delta k_L$).

APPENDIX B: CONDUCTANCE THROUGH A QUANTUM DOT USING PERTURBATION THEORY

In this appendix, we sketch the derivation of the equation (46). We follow Ref. [25] and first derive a perturbative expression for the current assuming there is a small difference of potential $eV = \mu_L - \mu_R$ between the left and right reservoir. The current operator between the left and right side of the dot can be expressed as:

$$\hat{I}(t) = \frac{ie}{\hbar} \int d\epsilon d\epsilon' f_L^*(\epsilon) f_R(\epsilon') \left(J_{LR} c_{L,\epsilon}^\dagger \frac{\vec{\sigma}}{2} \cdot \vec{S}_{c_{R,\epsilon'}} + V_{LR} c_{L,\epsilon}^\dagger c_{R,\epsilon'} - H.c. \right) \quad (B1)$$

The current $\langle \hat{I} \rangle$ can be for example calculated using

$$\langle \hat{I} \rangle = \langle 0 | S(-\infty, 0) \hat{I}(0) S(0, -\infty) | 0 \rangle \quad (B2)$$

with

$$S(0, -\infty) = T_K e^{-\frac{i}{\hbar} \int_{-\infty}^0 dt H_{int}(t)}$$

where H_{int} contains the Kondo couplings plus the potential scattering terms (see Eq. (15)). T_K indicates the time ordering operator along a Keldysh contour and $|0\rangle$ designs the ground state at time $t = -\infty$. At second order, we simply pick up the commutator between the current operator and the interacting Hamiltonian

$$\langle \hat{I} \rangle^{(2)} = \frac{2e}{\hbar^2} R e \left\{ \int d\epsilon d\epsilon' f_L^*(\epsilon) f_R(\epsilon') \int_{-\infty}^0 \langle 0 | \left[J_{LR} c_{L,\epsilon}^\dagger(0) \frac{\vec{\sigma}}{2} \cdot \vec{S}_{c_{R,\epsilon'}}(0) + V_{LR} c_{L,\epsilon}^\dagger(0) c_{R,\epsilon'}(0), H_{int}(t) \right] | 0 \rangle \right\} \quad (B3)$$

Only the J_{LR} and V_{LR} terms give contributions. After performing the Wick contractions and taking the small V limit to extract the linear conductance, we recover the second order contributions to the expression in Eq. (15).

The calculation of the third order terms goes along the same line. By expanding both S operators to second order, we obtain three sorts of terms: a cross term mixing the first order expansions of $S(-\infty, 0)$ and $S(0, -\infty)$ (we denote this term $I_1^{(3)}$) and two other terms coming from the second order expansion of $S(0, -\infty)$ (denoted $I_2^{(3)}$) and from the second order expansion of $S(-\infty, 0)$ (denoted $I_3^{(3)}$).

Focusing first on the Kondo terms, the only possible contributions at third order are in $J_{LR}^2 J_{LL}$ and $J_{LR}^2 J_{RR}$. Let us calculate for example the terms in $J_{LR}^2 J_{RR}$. The mixed term in J_{RR} reads:

$$\begin{aligned} I_{1,R}^{(3)} = & -\frac{2e}{\hbar^3} J_{LR}^2 J_{RR} \int \int \int d\epsilon d\epsilon' d\omega \text{Im} \left\{ \rho^L(\epsilon) \rho^R(\epsilon') \rho^R(\omega) \int \int dt_1 dt_2 \langle S^a(t_1) S^b(0) S^c(t_2) \rangle \text{Tr} \left(\frac{\sigma^a}{2} \frac{\sigma^b}{2} \frac{\sigma^c}{2} \right) \right. \\ & \left(\langle c_{L,\epsilon}(t_1) c_{L,\epsilon}^\dagger(0) \rangle \langle c_{R,\epsilon'}(0) c_{R,\epsilon'}^\dagger(t_2) \rangle \langle c_{R,\omega}(t_1) c_{R,\omega}(t_2) \rangle \right. \\ & \left. \left. + \langle c_{R,\epsilon'}^\dagger(t_1) c_{R,\epsilon'}(0) \rangle \langle c_{L,\epsilon}^\dagger(0) c_{L,\epsilon}(t_2) \rangle \langle c_{R,\omega}(t_1) c_{R,\omega}^\dagger(t_2) \rangle \right) \right\} \quad (B4) \end{aligned}$$

Note that no time ordering is necessary here since the crossed terms belong to two different branches of the contour. Using $\langle S^a(t_1) S^b(0) S^c(t_2) \rangle = \frac{i}{8} \varepsilon^{abc}$ and $\text{Tr} \left(\frac{\sigma^a}{2} \frac{\sigma^b}{2} \frac{\sigma^c}{2} \right) = \frac{i}{4} \varepsilon^{abc}$ (where ε^{abc} is the antisymmetric unit tensor), and performing the two time integrations, we can easily evaluate this expression. The final result reads:

$$\begin{aligned} I_{1,R}^{(3)} = & \frac{2e}{\hbar} \frac{6\pi}{32} J_{LR}^2 J_{RR} \int d\epsilon \int d\epsilon' \left\{ PP \frac{\rho^L(\epsilon) (\rho^R(\epsilon'))^2}{\epsilon - \epsilon'} n_{\epsilon'}^R (1 - n_{\epsilon'}^R) \right. \\ & \left. + PP \frac{\rho^L(\epsilon) \rho^R(\epsilon) \rho^R(\epsilon')}{\epsilon - \epsilon'} (n_{\epsilon'}^R - n_{\epsilon'}^R (n_{\epsilon}^L + n_{\epsilon'}^R) + n_{\epsilon}^L n_{\epsilon'}^R) \right\}, \quad (B5) \end{aligned}$$

where $n^{L/R}$ is the occupation number in the left/right reservoir and PP stands for principal part.

We can perform similar calculations for the two other terms denoted $I_{2,R}$ and $I_{3,R}$ paying attention to the different time ordering. We give directly the final expressions for these two terms:

$$\begin{aligned} I_{1,R}^{(3)} = & -\frac{2e}{\hbar} \frac{6\pi}{32} J_{LR}^2 J_{RR} \int d\epsilon \int d\epsilon' \left\{ PP \frac{\rho^L(\epsilon) (\rho^R(\epsilon'))^2}{\epsilon - \epsilon'} n_{\epsilon}^L n_{\epsilon'}^R (1 - n_{\epsilon'}^R) \right. \\ & \left. + PP \frac{\rho^L(\epsilon) \rho^R(\epsilon) \rho^R(\epsilon')}{\epsilon - \epsilon'} n_{\epsilon}^L (1 - n_{\epsilon}^R) (2 - 3n_{\epsilon'}^R) \right\}, \quad (B6) \end{aligned}$$

and

$$I_{1,R}^{(3)} = -\frac{2e}{\hbar} \frac{6\pi}{32} J_{LR}^2 J_{RR} \int d\epsilon \int d\epsilon' \left\{ PP \frac{\rho^L(\epsilon)(\rho^R(\epsilon'))^2}{\epsilon - \epsilon'} (1 - n_\epsilon^L) n_{\epsilon'}^R (1 - n_{\epsilon'}^R) \right. \\ \left. + PP \frac{\rho^L(\epsilon)\rho^R(\epsilon)\rho^R(\epsilon')}{\epsilon - \epsilon'} n_\epsilon^R (1 - n_\epsilon^L) (3n_{\epsilon'}^R - 1) \right\}, \quad (B7)$$

Adding this three contributions, we find that the terms in $\rho^L(\epsilon)(\rho^R(\epsilon'))^2$ cancel out. The terms in $J_{LR}^2 J_{LL}$ can be read out directly by exchanging $L \leftrightarrow R$. For small voltage, we use $n^L(\epsilon) - n^R(\epsilon) = eV(-dn/d\epsilon)$ which provides the linear conductance given in Eq. (15).

A priori, one may expect other contributions at third order. The terms in $V_{LR}^2 J_{LL}$ and $V_{LR}^2 J_{RR}$ are trivially 0. One can also prove by a similar calculation that the terms in $J_{LR}^2 V_{LL}$ and $J_{LR}^2 V_{RR}$ involve no logarithm divergencies but instead the integral $PP \int d\epsilon' \rho^{L/R}(\epsilon')/(\epsilon - \epsilon')$, an integral which is zero in the continuum limit with $D_0 \rightarrow \infty$. The pure scattering contributions in $V_{LR}^2 V_{LL}$ and $V_{LR}^2 V_{RR}$ involve the same integral and therefore do not contain logarithmic divergences as it should be. These terms are negligible in the infrared limit since they do not renormalize as opposed to the terms involving only the Kondo couplings.

APPENDIX C: CONDUCTANCE THROUGH A RESONANT NON INTERACTING QUANTUM DOT CONNECTED TO FINITE SIZE WIRES

In this appendix, we calculate the conductance through the device depicted in Figure 1 when the quantum dot is modeled by a non interacting resonant level. It corresponds to $U = 0$ in (3). Generalizing (A6) to an asymmetric geometry. the transmission amplitude through the system

$$T_{tot}^{lr}(k) = \frac{T_{LW}^{lr} T_{WL}^{lr} T_0^{lr}}{1 - R_0^l R_{LW}^r e^{2ik_L d_L} - R_0^r R_{WL}^l e^{2ik_R d_R} + R_{LW}^r R_{WL}^l (R_0^l R_0^r - T_0^{lr} T_0^{rl}) e^{2ik_L d_L + k_R d_R}} \quad (C1)$$

where R_{LW}^r is reflection coefficient for the left weak link (connecting the left lead to the wire) for a wave coming from the right. R_{WL}^l is the opposite. T_{LW}^{lr} is the transmission coefficient through the left weak link for an electron coming from the lead (from left to right), T_{WL}^{lr} is the same for the right weak link, and finally $R_O^r, R_O^l, T_O^{lr}, T_O^{rl}$ are the 4 reflection and transmission coefficients through the central weak link. We write

$$T_0^{lr} = t_0 e^{i\varphi_0 + 3i\pi/2} ; \quad R_0^r = r_0 e^{i(\varphi_0 + \theta_0)} ; \quad R_0^l = r_0 e^{i(\varphi_0 - \theta_0)} \quad (C2)$$

with

$$t_0^2 = \frac{4(t_{WD}^L)^2 (t_{WD}^R)^2 \sin^2 k_L}{(\epsilon_0 + \cos k_L + \cos k_R - (t_{WD}^L)^2 \cos k_L - (t_{WD}^R)^2 \cos k_R)^2 + ((t_{WD}^L)^2 \sin k_L + (t_{WD}^R)^2 \sin k_R)^2} \quad (C3)$$

$$r_0^2 = \frac{(\epsilon_0 + \cos k_L + \cos k_R - (t_{WD}^L)^2 \cos k_L - (t_{WD}^R)^2 \cos k_R)^2 + ((t_{WD}^L)^2 \sin k_L - (t_{WD}^R)^2 \sin k_R)^2}{(\epsilon_0 + \cos k_L + \cos k_R - (t_{WD}^L)^2 \cos k_L - (t_{WD}^R)^2 \cos k_R)^2 + ((t_{WD}^L)^2 \sin k_L + (t_{WD}^R)^2 \sin k_R)^2} \quad (C4)$$

and

$$\varphi_0 = \arctan \left(\frac{(t_{WD}^L)^2 \sin k_L + (t_{WD}^R)^2 \sin k_R}{\epsilon_0 + \cos k_L + \cos k_R - (t_{WD}^L)^2 \cos k_L - (t_{WD}^R)^2 \cos k_R} \right) \quad (C5)$$

$$\theta_0 = \arctan \left(\frac{(t_{WD}^L)^2 \sin k_L - (t_{WD}^R)^2 \sin k_R}{\epsilon_0 + \cos k_L + \cos k_R - (t_{WD}^L)^2 \cos k_L - (t_{WD}^R)^2 \cos k_R} \right) \quad (C6)$$

$$(C7)$$

Using

$$T_{LW}^{lr} = \frac{2i\gamma_L \sin k e^{i(k-k_L)}}{\cos k_L - \gamma_L^2 \cos k - i(\sin k_L + \gamma_L^2 \sin k)} ; \quad R_{LW}^r = -\frac{\cos k_L - \gamma_L^2 \cos k + i(\sin k_L - \gamma_L^2 \sin k)}{\cos k_L - \gamma_L^2 \cos k - i(\sin k_L + \gamma_L^2 \sin k)} ; \quad (C8)$$

$$T_{WL}^{lr} = \frac{2i\gamma_R \sin k_R e^{-i(k-k_R)}}{\cos k_R - \gamma_R^2 \cos k - i(\sin k_R + \gamma_R^2 \sin k)} ; \quad R_{WL}^l = -\frac{\cos k_R - \gamma_R^2 \cos k + i(\sin k_R - \gamma_R^2 \sin k)}{\cos k_R - \gamma_R^2 \cos k - i(\sin k_R + \gamma_R^2 \sin k)} ; \quad (C9)$$

and the property $R_0^l R_0^r - T_0^{lr} T_0^{rl} = e^{2i\varphi_0}$, the expression (C1) can be worked out easily. The final result reads

$$|T_{tot}|^2 = \frac{(2t_0\gamma_L\gamma_R \sin k \sin k_R)^2}{C^2 + D^2} \quad (\text{C10})$$

with

$$\begin{aligned} C = & \cos(k_L d_L + k_R d_R + \varphi_0) (\cos(k_L + k_R) + \gamma_L^2 \gamma_R^2 \cos 2k - \gamma_L^2 \cos k_R \cos k - \gamma_R^2 \cos k_L \cos k) \\ & - r_0 \cos(k_R d_R + \theta_0 - k_L d_L) (\cos(k_L + k_R) + \gamma_L^2 \gamma_R^2 - \gamma_L^2 \cos k_R \cos k - \gamma_R^2 \cos k_L \cos k) \\ & - \sin(k_L d_L + k_R d_R + \varphi_0) (\sin(k_L + k_R) - \gamma_L^2 \sin k_R \cos k - \gamma_R^2 \sin k_L \cos k) \\ & - r_0 \sin(k_R d_R + \theta_0 - k_L d_L) (\sin(k_L - k_R) - \gamma_L^2 \sin k_R \cos k + \gamma_R^2 \sin k_L \cos k) \end{aligned} \quad (\text{C11})$$

and

$$\begin{aligned} D = & -\cos(k_L d_L + k_R d_R + \varphi_0) \sin k (\gamma_R^2 \cos k_L + \gamma_L^2 \cos k_R - 2\gamma_R^2 \gamma_L^2 \cos k) \\ & r_0 \cos(k_R d_R + \theta_0 - k_L d_L) \sin k (\gamma_R^2 \cos k_L - \gamma_L^2 \cos k_R) \\ & + \sin(k_L d_L + k_R d_R + \varphi_0) \sin k (\gamma_R^2 \cos k_L + \gamma_L^2 \cos k_R) \\ & - r_0 \sin(k_R d_R + \theta_0 - k_L d_L) \sin k (\gamma_R^2 \sin k_L - \gamma_L^2 \sin k_R) \end{aligned} \quad (\text{C12})$$

Acknowledgments We would like to acknowledge interesting discussions with Carlos Balseiro, Claudio Chamon, Leonid Glazman and Mark Kastner. During the course of

this work PS has been partially supported by the Swiss NSF, NCCR, and the EU RTN Spintronics No HPRN-CT-2002-00302. IA was supported by the NSF grant DMR-0203159.

* Electronic address: pascal.simon@grenoble.cnrs.fr

† Electronic address: affleck@physics.bu.edu

¹ D. Goldhaber-Gordon, H. Shtrikman, D. Mahalu, D. Abusch-Magder, U. Meirav and M.A. Kaster, *Nature* **391**, 156 (1998).

² S.M. Cronewett, T.H. Oosterkamp, L.P. Kouwenhoven, *Science* **281**, 540 (1998); F. Simmel, R.H. Blick, U.P. Kotthaus, W. Wegscheider, M. Blichler, *Phys. Rev. Lett.* **83**, 804 (1999).

³ W.G. van der Wiel, S. De Franceschi, T. Fujisawa, J.M. Elzerman, S. Tarucha and L.P. Kouwenhoven, *Science*, **289**, 2105 (2000).

⁴ J. Nygard, D. H. Cobden, P. E. Lindelof, *Nature* **408**, 342 (2000).

⁵ Y. Ji, M. Heiblum, D. Sprinzak, D. Mahalu and H. Shtrikman, *Science* **290**, 779 (2000).

⁶ U. Gerland, J. von Delft, T. A. Costi, and Y. Oreg *Phys. Rev. Lett.* **84**, 3710 (2000).

⁷ O. Entin-Wohlman, A. Aharony, Y. Imry, Y. Levinson, and A. Schiller *Phys. Rev. Lett.* **88**, 166801 (2002); A. Aharony, O. Entin-Wohlman, B. I. Halperin, and Y. Imry, *Phys. Rev. B* **66**, 115311 (2002)

⁸ I. Affleck and P. Simon, *Phys. Rev. Lett.* **86**, 2854 (2001).

⁹ P. Simon and I. Affleck, *Phys. Rev.* **B64**, 085308 (2001).

¹⁰ H. Hu, G.-M. Zhang and Yu Lu, *Phys. Rev. Lett.* **86**, (2001).

¹¹ H.-P. Eckle, H. Johannesson, and C. A. Stafford *Phys. Rev. Lett.* **87**, 016602 (2001) *Phys. Rev. Lett.* **82**, 5088 (1999).

¹² K. Kang and S.-C. Shin, *Phys. Rev. Lett.* **85**, 5619 (2000).

¹³ V. Ferrari, G. Chiappe, E.V. Anda and M.A. Davidovich, *Phys. Rev. Lett.* **82**, 5088 (1999).

¹⁴ A. A. Aligia, *Phys. Rev.* **B 66**, 165303 (2002)

¹⁵ I. Affleck and P. Simon, *Phys. Rev. Lett.* **88**, 139701 (2002); H.-P. Eckle, H. Johannesson, and C. A. Stafford, *Phys. Rev. Lett.* **88**, 139702 (2002).

¹⁶ E. Sorensen and I. Affleck, unpublished.

¹⁷ W. B. Thimm, J. Kroha and J. von Delft, *Phys. Rev. Lett.* **82** 2143 (1999).

¹⁸ P. S. Cornaglia and C. A. Balseiro, *Phys. Rev.* **B66**, 115303 (2002); *ibid* **B66**, 174404 (2002).

¹⁹ K. Kang and L. Craco, *Phys. Rev. B* **65**, 033302 (2002).

²⁰ P. Simon and I. Affleck, *Phys. Rev. Lett.* **89** 206602 (2002).

²¹ P. S. Cornaglia and C. A. Balseiro, *cond-mat/0212119*.

²² S. Y. Cho, H-Q. Zhou and R. H. McKenzie, *cond-mat/0302090*.

²³ T. K. Ng and P. A. Lee, *Phys. Rev. Lett.* **61** 1768 (1988).

²⁴ D. C. Langreth, *Phys. Rev.* **150** 516 (1966).

²⁵ A. Kaminski, Yu. V. Nazarov and L. I. Glazman, *Phys. Rev.* **B 62**, 8154 (2000).

²⁶ A. C. Hewson, *The kondo Problem to Heavy Fermions* (Cambridge University Press, Cambridge, UK, 1997), chap 7.

²⁷ P. Nozières, *Proceedings of the 14th International Conference on Low Temperature Physics*, (ed. M. Krusius and M. Vuorio, North-Holland, Amsterdam, 1975), Vol. 5, p. 339.

²⁸ S. Kettemann and M. E. Raikh, *Phys. Rev. Lett.* **90** 146601 (2003).

²⁹ K. A. Matveev, L. I. Glazman and H. U. Baranger, *Phys. Rev. B* **53** 1034 (1996); *ibid* **B 54** 5637 (1996).